TITLE

An important role for triglyceride in regulating spermatogenesis

AUTHORS

Charlotte F. Chao[1&], Yanina-Yasmin Pesch[1&], Huaxu Yu[2], Chenjingyi Wang[2], Maria J. Aristizabal[3], Tao Huan[2], Guy Tanentzapf[1], Elizabeth J. Rideout[1*]

AFFILIATIONS

[1] Department of Cellular and Physiological Sciences, Life Sciences Institute, The University of British Columbia, Vancouver, BC, Canada V6T 1Z3

[2] Department of Chemistry, The University of British Columbia, Vancouver, BC, Canada V6T 1Z1

[3] Department of Biology, Queen's University, Kingston, ON, Canada K7L 3N6

* Corresponding author

[&] Equally contributing authors

[*] Correspondence: elizabeth.rideout@ubc.ca

ABSTRACT

Drosophila is a powerful model to study how lipids affect spermatogenesis. Yet, the contribution of neutral lipids, a major lipid group which resides in organelles called lipid droplets (LD), to sperm development is largely unknown. Emerging evidence suggests LD are present in the testis and that loss of neutral lipid- and LD-associated genes causes subfertility; however, key regulators of testis neutral lipids and LD remain unclear. Here, we show LD are present in early-stage somatic and germline cells within the *Drosophila* testis. We identified a role for triglyceride lipase *brummer* (*bmm*) in regulating testis LD, and found that whole-body loss of *bmm* leads to defects in sperm development. Importantly, these represent cell-autonomous roles for *bmm* in regulating testis LD and spermatogenesis. Because lipidomic analysis of *bmm* mutants revealed excess triglyceride accumulation, and spermatogenic defects in *bmm* mutants were rescued by genetically blocking triglyceride synthesis, our data suggest that *bmm*-mediated regulation of triglyceride influences sperm development. This identifies triglyceride as an important neutral lipid that contributes to *Drosophila* sperm development, and reveals a key role for *bmm* in regulating testis triglyceride levels during spermatogenesis.

KEYWORDS

Triglyceride, lipid droplet, spermatogenesis, testis, *brummer*, adipose triglyceride lipase (ATGL), lipidomics.

INTRODUCTION

Lipids play an essential role in regulating spermatogenesis across animals [1–4]. Studies in *Drosophila* have illuminated key roles for multiple lipid species in regulating sperm development [5–7]. For example, phosphatidylinositol and its phosphorylated derivatives participate in diverse aspects of *Drosophila* spermatogenesis including meiotic cytokinesis [1,8–11], somatic cell differentiation [12], germline and somatic cell polarity maintenance [13–16], and germline stem cell (GSC) maintenance and proliferation [17]. Membrane lipids also influence sperm development [18,19], whereas fatty acids play a role in processes such as meiotic cytokinesis [20] and sperm individualization [21,22]. While these studies suggest key roles for membrane lipids and fatty acids during *Drosophila* spermatogenesis, some of which are conserved in mammals [23–25], much less is known about how neutral lipids contribute to spermatogenesis.

Neutral lipids are a major lipid group that includes triglyceride and cholesterol ester, and reside within specialized organelles called lipid droplets (LD) [26]. LD are found in diverse cell types (*e.g*. adipocytes, muscle, liver, glia, neurons) [27,28,26], and play key roles in maintaining cellular lipid homeostasis. In nongonadal cell types, correct regulation of LD contributes to cellular energy production [29–31], sequestration and redistribution of lipid precursors [32–36], and regulation of lipid toxicity [37–39]. The importance of LD to normal cellular function in nongonadal cell types is shown by the fact that dysregulation of LD causes defects in cell differentiation, survival, and energy production [26,37,40,41]. In the testis, much less is known about the regulation and function of neutral lipids and LD, and how this regulation affects sperm development.

62 Multiple lines of evidence suggest a potential role for neutral lipids and LD during
63 spermatogenesis. First, genes that encode proteins associated with neutral lipid
64 metabolism and LD are expressed in the testis across multiple species [42–44].
65 Second, testis LD have been identified in mammals and flies under both normal
66 physiological conditions [27,44–48] and after mitochondrial stress [49]. Third, loss of
67 genes associated with neutral lipid metabolism and LD cause subfertility phenotypes in
68 both flies and mammals [27,50–52]. While studies suggest that mammalian testis LD
69 contribute to steroidogenesis [53,54], the spatial, temporal, and cell-type specific
70 requirements for neutral lipids and LD in the testis have not been explored in detail in
71 any animal. It remains similarly unclear which genes are responsible for regulating
72 neutral lipids and LD during spermatogenesis.
73 To address these knowledge gaps, we used *Drosophila* to investigate the
74 regulation and function of neutral lipids and LD during sperm development. Our detailed
75 analysis of spermatogenesis under normal physiological conditions revealed the
76 presence of LD in early-stage somatic and germline cells in the testis. We identified
77 triglyceride lipase *brummer* (*bmm*) as a regulator of testis LD, and showed that this
78 represents a cell-autonomous role for *bmm* in the germline. Importantly, we found that
79 *bmm*-mediated regulation of testis LD was significant for spermatogenesis, as both
80 whole-body and cell-autonomous loss of *bmm* caused defects in sperm development.
81 Given that our lipidomic analysis revealed an excess accumulation of triglyceride in
82 animals lacking *bmm*, and that genetically blocking triglyceride synthesis rescued many
83 spermatogenic defects associated with *bmm* loss, our data suggests that *bmm*-
84 mediated regulation of triglyceride is important for normal *Drosophila* sperm

85 development. This reveals previously unrecognized roles for neutral lipids such as
86 triglyceride in regulating spermatogenesis, and for *bmm* in regulating sperm
87 development under normal physiological conditions. Together, these findings advance
88 knowledge of the regulation and function of neutral lipids during spermatogenesis.
89

90 **RESULTS**

91 **Lipid droplets are present in early-stage somatic and germline cells**

92 We previously reported the presence of small LD (<1 μm) at the apical tip of the testis
93 [27], a finding we reproduced in w^{1118} males using neutral lipid stain BODIPY (Figure
94 1A). These LD were present in the region that contains stem cells, early-stage somatic
95 cells, and germline cells (Figure 1A-A', arrows). LD were also present in the hub, an
96 organizing center and stem cell niche in the *Drosophila* testis (Figure 1A"-A"', arrows)
97 [55], but largely absent within the area occupied by spermatocytes (Figure 1A and A',
98 arrowheads). This LD distribution was reproduced in two independent genetic
99 backgrounds and at two additional ages (Figure 1B, 1C). While LD may contain multiple
100 neutral lipid species [56], cholesterol-binding fluorescent polyene antibiotic filipin III did
101 not detect cholesterol within testis LD (Figure S1A), suggesting triglyceride is the main
102 neutral lipid in *Drosophila* testis LD.

103 *Drosophila* spermatogenesis requires the co-development and differentiation of
104 the germline and the somatic lineages [57]. To identify LD in each lineage, we used the
105 GAL4/UAS system to overexpress a GFP transgene fused to the LD-targeting motif of
106 motor protein *Klarsicht* (*UAS-GFP-LD*) [58]. Somatic overexpression of *UAS-GFP-LD*
107 using *Traffic jam (Tj)-GAL4* revealed that the majority of somatic LD in 0-day-old males

108 were located <30 μm from the hub (Figure 1D, 1E). Because the somatic LD distribution
109 coincided with a marker for somatic stem cells and their immediate daughter cells (Zinc
110 finger homeodomain 1, Zfh-1) (Figure 1F; two-sample Kolmogorov-Smirnov test) [59],
111 but not with a marker for late somatic cells (Eyes absent, Eya) [12,60], our data suggest
112 LD are present in early somatic cells. Germline overexpression of *UAS-GFP-LD* using
113 *nanos (nos)-GAL4* demonstrated the presence of LD within germline cells near the
114 apical tip of the testis in 0-day-old males (Figure 1G, 1H). Specifically, the
115 disappearance of germline LD coincided with peak expression of a GFP reporter that
116 reflects the expression of Bag-of-marbles (Bam) protein in the testis (Bam-GFP) [61]
117 (Figure 1I, 1J). Because peak Bam expression signals the last round of transient
118 amplifying mitotic cell cycle prior to the germline's transition into the meiotic cell cycle
119 [62–64], our data suggests that germline LD, like somatic LD, are present in cells at
120 early stages of development.
121

122 **_brummer_ plays a cell-autonomous role in regulating testis lipid droplets**

123 *Adipose triglyceride lipase* (*ATGL*) is a critical regulator of neutral lipid metabolism and
124 LD [65–74]. Loss of *ATGL* in many cell types triggers LD accumulation, and *ATGL*
125 overexpression decreases LD number [30,67,68,71,73,75,76]. Given that the
126 *Drosophila ATGL* homolog *brummer* (*bmm*) regulates testis LD induced by
127 mitochondrial stress [49], we explored whether *bmm* regulates testis LD under normal
128 physiological conditions. We first examined *bmm* expression in the testis by isolating
129 this organ from flies carrying a *bmm* promoter-driven *GFP* transgene (*bmm-GFP*) that
130 recapitulates many aspects of *bmm* mRNA regulation [77]. GFP expression was present

131 in the germline of *bmm-GFP* testes, and we found germline GFP levels were higher in
132 spermatocytes than at earlier stages of sperm development (Figure 2A, 2B; one-way
133 ANOVA with Tukey multiple comparison test). In further support of this observation, we
134 analyzed a publicly available single-cell RNA sequencing dataset from the male
135 reproductive organ [78]. Using pseudotime analysis, we arranged the germline (Figure
136 S2A) and somatic cells (Figure S2B) based on their annotated developmental trajectory.
137 The expression pattern of *bmm* in the germline matched our observation with the *bmm-*
138 *GFP* reporter (Figure S2C). While levels of the *bmm-GFP* reporter were low in somatic
139 cells, single-cell RNA sequencing data identified *bmm* expression in the somatic
140 lineage, with higher expression in cells at later stages of development (Figure S2D).
141 Additional neutral lipid- and lipid droplet-associated genes such as *lipid storage droplet-*
142 *2*, *Seipin*, *Lipin*, and *midway* also showed differential regulation during differentiation in
143 the testis (Figure S2C, S2D). Combined with our data on the location of testis LD, these
144 gene expression data suggest that *bmm* upregulation in both somatic and germline cells
145 during differentiation corresponds to the downregulation of testis LD. Supporting this,
146 germline GFP levels were negatively correlated with testis LD in *bmm-GFP* flies (Figure
147 2A, 2C), suggesting regions with higher *bmm* expression had fewer LD.
148 To test whether *bmm* regulates testis LD, we compared LD in testes from 0-day-
149 old males carrying a loss-of-function mutation in *bmm* (bmm^{1}) to control male testes
150 (bmm^{rev}) [67]. bmm^{1} males had significantly more LD across all LD sizes compared with
151 control males at the apical tip of the testis (Figure 2D–2G; Welch two-sample t-test with
152 Bonferroni correction) and showed a significantly expanded LD distribution (Figure 2D–
153 2F, 2H; two-sample Kolmogorov-Smirnov test). This suggests *bmm* normally restricts

154 LD to the apical tip of the testis, an observation we confirmed in both somatic and
155 germline lineages using lineage-specific expression of GFP-LD (Figure S3A–S3D).
156 Importantly, after inducing homozygous *bmm*^{rev} or *bmm*^{1} clones in the testes using the
157 *FLP-FRT* system (Figure 3A, 3B) [79], we found *bmm*^{1} spermatocyte clones had
158 significantly more LD at 3 days post-clone induction (Figure 3C; Welch two-sample t-
159 test), a stage at which LD were absent from *bmm*^{rev} clones. Because we observed no
160 significant effect of cell-autonomous *bmm* loss on LD at any other stage of germline
161 development (Figure 3C), this suggests *bmm* does not regulate LD at early stages of
162 germ cell development. Instead, our data suggest *bmm* plays a role in regulating LD at
163 the spermatogonia-spermatocyte transition. While we were unable to assess LD in
164 *bmm*^{1} somatic clones, our data reveals a previously unrecognized cell-autonomous role
165 for *bmm* as a key regulator of LD in germline cells.
166

167 ***brummer* plays a cell-autonomous role in regulating germline development**

168 To determine the physiological significance of *bmm*-mediated regulation of testis LD, we
169 investigated testis and sperm development in males without *bmm* function. In 0-day-old
170 *bmm*^{1} males reared at 25°C, testis size was significantly smaller than in age-matched
171 *bmm*^{rev} controls (Figure 4A, 4B; Welch two-sample t-test), and the number of spermatid
172 bundles was significantly lower (Figure 4C; Kruskal-Wallis rank sum test). When the
173 animals were reared at 29°C, a temperature that exacerbates spermatogenesis defects
174 associated with changes in lipid metabolism [21], *bmm*^{1} phenotypes were more
175 pronounced (Figure S3A, S3B; Welch two-sample t-test, Kruskal-Wallis rank sum test).
176 Defects in testis size were also observed at 14 days post-eclosion; suggesting testis

177 size defects persist later into the life course (Figure S4C; Welch two-sample t-test). In
178 contrast, the number of spermatid bundles per testis was not significantly different
179 between *bmm*^{1} and *bmm*^{rev} males at this age (Figure S4D; Welch two-sample t-test),
180 potentially due to a large decrease in the number of spermatid bundles in 14-day-old
181 *bmm*^{rev} males (Figure 4C, S4D). Together, these data suggest loss of *bmm* affects testis
182 development and spermatogenesis. Similar phenotypes are observed in male mice
183 without ATGL [52], and supplementing the diet of *bmm*^{1} males with medium-chain
184 triglycerides (MCT) partially rescues the testis and spermatogenic defects we observed
185 in flies (Figure S4E, S4F; one-way ANOVA with Tukey multiple comparison test), as it
186 does in mice [52,80]. This identifies similarities between flies and mice in fertility-related
187 phenotypes associated with whole-body loss of *bmm*/*ATGL.*
188 To explore spermatogenesis in *bmm*^{1} animals, we used an antibody against germ
189 cell-specific marker Vasa to visualize the germline in the testes of *bmm*^{1} and *bmm*^{rev}
190 males (Figure 4D, 4E) [81]. We observed a significant increase in the number of
191 germline stem cells (GSC) (Figure 4F; Kruskal-Wallis rank sum test) and higher
192 variability in GSC number in *bmm*^{1} males (p=5.7×10^{-12} by F-test). Given that GSC
193 number is affected by hub size and GSC proliferation [82,83], we monitored both
194 parameters in *bmm*^{1} and *bmm*^{rev} controls. While hub size in *bmm*^{1} testes was
195 significantly larger than in testes from *bmm*^{rev} controls (Figure S4G, S4H; Welch two-
196 sample t-test), the number of phosphohistone H3-positive GSCs, which indicates
197 proliferating GSCs, was unchanged in *bmm*^{1} animals (Figure S4I; Kruskal-Wallis rank
198 sum test). While this indicates a larger hub may partly explain *bmm'*s effect on GSC
199 number, *bmm* also plays a cell-autonomous role in regulating GSCs, as we recovered a

200 higher proportion of *bmm*^{1} clones in the GSC pool compared with *bmm*^{rev} clones at 14
201 days after clone induction (Figure 4G; Welch two-sample t-test). Given that we detected
202 no effect of cell-autonomous *bmm* loss on the number of GSC LD (Figure 3C), more
203 work will be needed to understand how *bmm* regulates GSCs at a stage prior to its
204 effects on LD number. Future studies will also need to confirm whether *bmm*^{1} mutant
205 GSCs show an increased ability to occupy space at the hub.

206 Beyond GSCs, we uncovered additional spermatogenesis defects in *bmm*^{1}
207 testes. Peak Bam-GFP expression in germline cells of the testes from 0-day-old *bmm*^{1}
208 and *bmm*^{rev} males showed GFP-positive cysts were significantly further away from the
209 hub in *bmm*^{1} testes (Figure 4H, S4J; Welch two-sample t-test). Indeed, 15/18 *bmm*^{1}
210 testes contained Vasa-positive cysts with large nuclei in the distal half of the testis
211 (Figure 4I, arrows), a phenotype not present in *bmm*^{rev} testes (0/8) (p=0.0005 by
212 Pearson's Chi-square test). Because these phenotypes are also seen in testes with
213 differentiation defects [13,84], we recorded the stage of sperm development reached by
214 the germline in *bmm*^{1} testes. Most *bmm*^{1} testes contained post-meiotic cells in males
215 raised at 25°C (Figure S4K); however, germline development did not progress past the
216 spermatocyte stage in most *bmm*^{1} testes from animals raised at 29°C (Figure S4K).
217 Testes from *bmm*^{1} males reared at 25°C also had a smaller Boule-positive area (Figure
218 4J, S4L; Welch two-sample t-test), and fewer individualization complexes and waste
219 bags (Figure S4M, S4N; Kruskal-Wallis rank sum test). Because Boule-positive area,
220 individualization complexes, and waste bags indicate germline cells at later stages in
221 development, these data suggest the loss of *bmm* causes a reduction in differentiated
222 cell types. Because we observed significantly fewer *bmm*^{1} spermatocyte and spermatid

223 clones at 14 days after clone induction (Figure 4K, 4L; p = 0.0496, Kruskal-Wallis rank
224 sum test), these effects on germline development may represent a cell-autonomous role
225 for *bmm* in regulating spermatogenesis in this cell type. Given that the statistical
226 significance of this finding was not as strong as for our other data, future studies should
227 repeat this experiment with more samples. We also reveal a potential non-cell-
228 autonomous role for somatic *bmm*. While there was no difference in the ratio of Zfh-1-
229 positive cells between homozygous clones and heterozygous clones in animals carrying
230 the bmm^{1} or bmm^{rev} alleles at 14 days post clone induction (Figure S4O; Kruskal-Wallis
231 rank sum test), the distance from the hub to the Zfh-1 positive clones reside was
232 significantly decreased in bmm^{1} homozygous clones (Figure S4P; Kruskal-Wallis rank
233 sum test). Together, these data indicate *bmm* plays a cell-autonomous role in germline
234 cells, and potentially a non-cell-autonomous role in somatic cells, to regulate
235 spermatogenesis.
236
237 ***brummer*-dependent regulation of testis triglyceride levels affects**
238 **spermatogenesis**
239 *ATGL* catalyzes the first and rate-limiting step of triglyceride hydrolysis [73,85,86]. Loss
240 of this enzyme or its homologs leads to excess triglyceride accumulation
241 [27,30,67,73,75] and shifts in multiple lipid classes [66,87–89]. To determine how loss of
242 *bmm* affects spermatogenesis, we carried out whole-body mass spectrometry (MS)-
243 based untargeted lipidomic profiling of bmm^{1} and bmm^{rev} males. Hierarchical clustering
244 of lipid species suggests that bmm^{1} and bmm^{rev} males show distinct lipidomic profiles
245 (Figure 5A). Overall, we detected 2464 and 1144 lipid features with high quantitative

246 confidence in positive and negative ion modes, respectively. By matching experimental
247 *m/z*, isotopic ratio, and tandem MS spectra to lipid libraries, we confirmed 293 unique
248 lipid species (Supplemental table 1). We found 107 lipids had a significant change in
249 abundance between *bmm*^{1} and *bmm*^{rev} males (p_{adj}<0.05): 85 species were upregulated
250 in *bmm*^{1} males and 22 lipid species were downregulated. Among differentially regulated
251 species from different lipid classes, triglyceride had the largest residual above expected
252 proportion (p=5.00×10^{-4} by Pearson's Chi-squared test). This suggests triglyceride is the
253 lipid class most affected by loss of *bmm* (Figure 5B, 5C).

254 In *bmm*^{1} males, the majority of triglyceride species (55/97) were significantly
255 higher in abundance compared with *bmm*^{rev} control males. Because we observed a
256 positive correlation between the fold increase in triglyceride abundance with both the
257 number of double bonds (p=7.52×10^{-8} by Kendall's rank correlation test; Figure S5A)
258 and the number of carbons (p=2.77×10^{-10} by Kendall's rank correlation test; Figure
259 S5B), our data align well with *bmm*/*ATGL's* known role in regulating triglyceride levels
260 [67,68,73] and its substrate preference of long-chain polyunsaturated fatty acids [85].
261 While we also detected changes in species such as fatty acids, acylcarnitine, and
262 membrane lipids (Figure S5C–S5H), in line with recent *Drosophila* lipidomic data
263 [90,91], the striking accumulation of triglyceride in *bmm*^{1} males suggested that excess
264 testis triglyceride in *bmm*^{1} males may contribute to their spermatogenic defects. To test
265 this, we examined spermatogenesis in *bmm*^{1} males carrying loss-of-function mutations
266 in *midway* (*mdy*). *mdy* is the *Drosophila* homolog of *diacylglycerol O-acyltransferase 1*
267 (*DGAT1*), and whole-body loss of *mdy* reduces whole-body triglyceride levels [92–94].
268 Importantly, testes isolated from males with global loss of both *bmm* and *mdy*

269 (*mdy*$^{QX25/k03902}$;*bmm*^{1}) had fewer LD than testes dissected from *bmm*^{1} males (Figures
270 5D, S5I; one-way ANOVA with Tukey multiple comparison test).
271 We found that testes isolated from *mdy*$^{QX25/k03902}$;*bmm*^{1} males were significantly
272 larger and had more spermatid bundles than testes from *bmm*^{1} males (Figure 5E–G;
273 one-way ANOVA with Tukey multiple comparison test). The elevated number of GSCs
274 in *bmm*^{1} male testes was similarly rescued in *mdy*$^{QX25/k03902}$;*bmm*^{1} males (Figure 5H;
275 one-way ANOVA with Tukey multiple comparison test). These data suggest that
276 defective spermatogenesis in *bmm*^{1} males can be partly attributed to excess triglyceride
277 accumulation. Notably, at least some of the effects of global *mdy* loss on *bmm*^{1} males
278 can be attributed to the germline: RNAi-mediated knockdown of *mdy* in the germline of
279 *bmm*^{1} males partially rescued the defects in testis size (Figure 5I; Kruskal-Wallis rank
280 sum test with Dunn's multiple comparison test) and GSC variance (Figure S5J; p=4.5 x
281 10^{-5} and 8.2 x 10^{-3} by F-test from the GAL4- and UAS-only crosses, respectively). While
282 future studies will need to test whether germline-specific loss of *mdy* also rescues
283 spermatid number defects in *bmm*^{1} males, our data suggest *bmm*-mediated regulation
284 of testis triglyceride plays a previously unrecognized role in regulating sperm
285 development.
286
287 **DISCUSSION**
288 In this study, we used *Drosophila* to gain insight into how the neutral lipids, a major lipid
289 class, contribute to sperm development. We describe the distribution of LD under
290 normal physiological conditions in the *Drosophila* testis, and show that LD are present
291 at the early stages of development in both somatic and germline cells. While many

292 factors are known to regulate LD in nongonadal cell types, we reveal a cell-autonomous
293 role for triglyceride lipase *bmm* in regulating testis LD during spermatogenesis. In
294 particular, we identified a requirement for *bmm* in mediating the decrease in LD at the
295 spermatogonia-spermatocyte transition. This regulation is important for sperm
296 development, as our data indicates that loss of *bmm* causes a decrease in the number
297 of differentiated cell types in the testis. This phenotype may be attributed to a delay in
298 differentiation, a block in differentiation, or to a loss of differentiated cells through cell
299 death. Future studies will therefore be essential to resolve why *bmm* loss causes a
300 reduction in differentiated cell types. Nevertheless, these defects in the number of
301 differentiated cell types can be partially explained by the excess accumulation of
302 triglyceride in flies lacking *bmm*, as global and cell type-specific inhibition of triglyceride
303 synthesis rescues multiple spermatogenic defects in *bmm* mutants. Together, our data
304 reveals previously unrecognized roles for LD and triglycerides during spermatogenesis,
305 and for *bmm* as an important regulator of testis LD and germline development under
306 normal physiological conditions.

307 One key outcome of our study was increased knowledge of LD regulation and
308 function in the testis. Despite rapidly expanding knowledge of LD in cell types such as
309 adipocytes or skeletal muscle, less is known about how LD influence spermatogenesis
310 under normal physiological conditions. In mammals, testis LD contain cholesterol and
311 play a role in promoting steroidogenesis [95,96]. In flies, we show that LD are present in
312 the testis, and that excess accumulation of these LD affects sperm development. In
313 nongonadal cell types, triglycerides provide a rich source of fatty acids for cellular ATP
314 production, lipid building blocks to support membrane homeostasis and growth, and

315 metabolites that can act as signaling molecules [26]. Because ATP production, lipid
316 precursors, and lipid signaling all play roles in supporting normal sperm development
317 [97,98], future studies will need to determine how each of these processes is affected
318 when excess triglyceride accumulates in testis LD (Figure 6). It will also be important to
319 determine whether it is the loss of metabolites produced by *bmm*'s enzymatic action, or
320 an increase in triglycerides, that leads to the reduction in differentiated cell types during
321 spermatogenesis. Together, these experiments will provide critical insight into how
322 triglyceride stored within testis LD contributes to overall cellular lipid metabolism during
323 spermatogenesis. Because of the parallel spermatogenic defects we observed in *bmm*
324 mutants and *ATGL*-deficient mice, we expect these mechanisms will also operate in
325 other species.

326 A more comprehensive understanding of neutral lipid metabolism during sperm
327 development will also emerge from studies on the upstream signaling networks that
328 regulate testis LD and triglyceride. Given that we show an important and cell-
329 autonomous role for *bmm* in regulating testis LD and triglyceride, future studies will
330 need to identify factors that regulate *bmm* in the testis. Based on public single-cell
331 RNAseq data and the *bmm-GFP* reporter strain, our data suggest *bmm* mRNA levels
332 are differentially regulated between early and later stages of sperm development.
333 Candidates for mediating this regulation include the insulin/insulin-like growth factor
334 signaling pathway (IIS), Target of rapamycin (TOR) pathway, and nuclear factor
335 κB/Relish pathway (NFκB), as all of these pathways influence *bmm* mRNA levels in
336 nongonadal cell types [99–105]. Beyond mRNA levels, Bmm protein levels and post-
337 translational modifications may also be differentially regulating during spermatogenesis.

338 For example, studies show that the proteins encoded by *bmm* homologs in other
339 animals are regulated by phosphorylation [106], mediated by kinases such as
340 adenosine monophosphate-activated protein kinase (AMPK) and protein kinase A
341 (PKA) [107–109]. Importantly, many of these pathways, including IIS, TOR, AMPK,
342 NFκB and possibly PKA influence *Drosophila* sperm development [110–115]. Identifying
343 the signaling networks that influence *bmm* regulation during sperm development will
344 therefore lead to a deeper understanding of how testis LD and triglyceride are
345 coordinated with physiological factors to promote normal spermatogenesis. Because
346 pathways such as IIS and AMPK, and others, regulate sperm development in other
347 species [116–118], these insights may reveal conserved mechanisms that govern the
348 regulation of cellular neutral lipid metabolism during sperm development.
349
350
351

352 **ACKNOWLEDGEMENTS**

353 We thank Dr. Ronald Kühnlein for *bmm*^{1} and *bmm*^{rev} lines [67], Dr. Michael Welte for
354 *UAS-GFP-LD* [58], and Dr. Kaeko Kamei for *bmm-GFP* [77]. We used stocks from the
355 Bloomington *Drosophila* Stock Center (NIH P40OD018537) and Vienna *Drosophila*
356 Resource Center (VDRC). We acknowledge critical resources and information provided
357 by FlyBase [119] (supported by the National Human Genome Research Institute at the
358 U.S. National Institutes of Health (U41 HG000739) and the British Medical Research
359 Council (MR/N030117/1)). This work was supported by the Life Sciences Institutes
360 Imaging Core, supported by the UBC GREx Biological Resilience Initiative. Funding for
361 this study was provided by grants to EJR from the Canadian Institutes for Health
362 Research (PJT-153072), Michael Smith Foundation for Health Research (16876), and
363 the Canadian Foundation for Innovation (JELF-34879). GT was supported by a grant
364 from the Natural Sciences and Engineering Research Council (NSERC; 2018-04648),
365 TH/HY/CW were supported by NSERC (2020-04895), MA was supported by the
366 Jacob's foundation. We would like to acknowledge that our research takes place on the
367 traditional, ancestral, and unceded territory of the Musqueam people; a privilege for
368 which we are grateful.

369

370 **AUTHOR CONTRIBUTIONS**

371 Conceptualization, C.C. and E.J.R.; Methodology, C.C. and Y.Y.P.; Software, C.C.;
372 Investigation, C.C., H.Y., and Y.Y.P.; Lipidomics, M.A., H.Y., C.W., T.H.; Writing –
373 Original Draft, C.C. and E.J.R.; Writing – Review and Editing, C.C., E.J.R., and Y.Y.P.;

374 Supervision, E.J.R., G.T., and T.H.; Project administration, E.J.R.; Funding Acquisition,
375 E.J.R., G.T., and T.H.
376
377 **DECLARATION OF INTERESTS**
378 The authors declare no competing interests.
379
380 **FIGURE LEGENDS**
381 **Figure 1 – Lipid droplets are present in early-stage somatic and germ cells.** (A)
382 Testis lipid droplets (LD) in *w*^{1118} animals visualized with neutral lipid dye BODIPY.
383 (A,A') Scale bar=50 μm; (A'',A''') scale bar=15 μm. Asterisk indicates hub in all images.
384 Arrows point to LD; arrowheads point to spermatocytes in A,B. Spermatocytes were
385 identified as described in methods section. (B) Testis LD visualized with BODIPY in
386 newly-eclosed males from two wild-type genotypes. Scale bars: main image=50 μm;
387 inset image=10 μm. (C) Testis LD from *w*^{1118} animals at different times post-eclosion.
388 Scale bars=50 μm. (D) Testis LD visualized with LipidTox Red in animals with somatic
389 cell overexpression of GFP-LD (*Tj-GAL4>UAS-GFP-LD*). GFP- and LipidTox Red-
390 positive punctae are somatic LD (D–D'' arrows); LipidTox punctae without GFP indicate
391 germline LD (D–D'' arrowheads). Scale bars=10 μm. (E) Histogram showing the spatial
392 distribution of somatic cell LD; error bars represent standard error of the mean (SEM).
393 (F) Cumulative frequency distributions of somatic LD (blue line, data reproduced from
394 E), zfh-1-positive somatic cells (zfh-1^{+} cells, orange line), and Eya-positive somatic cells
395 (Eya^{+} cells, grey line). (G) Testis LD visualized with LipidTox Red in males with germline
396 overexpression of GFP-LD (*nos-GAL4>UAS-GFP-LD*). GFP- and LipidTox Red-positive

397 punctae indicate germline LD (arrows); LipidTox punctae without GFP indicate non-
398 germline LD (arrowheads). Scale bars=10 μm. (H) Histogram representing the spatial
399 distribution of LD within the germline; error bars represent SEM. (I) Histogram
400 representing the spatial distribution of LD and GFP fluorescence (green line) (arbitrary
401 units, a.u.) in a representative testis of a *bam-GFP* animal (panel J). (J) Testis LD in a
402 *bam-GFP* animal; arrows point to LD and arrowheads point to spermatocytes. Scale
403 bar=50 μm. See also Supplemental Figure 1.
404
405 **Figure 2 – *brummer* regulates lipid droplets in both germline and somatic cells of**
406 **the testis.** (A-A'''') Testis lipid droplets (LD) indicated by LipidTox Red in *bmm-GFP*
407 animals. Arrows point to LD in all images. Arrowheads point to spermatocytes. Scale
408 bars=50 μm. Asterisks indicate the hub in all images. (B) Quantification of nuclear GFP
409 intensity in testes isolated from *bmm-GFP* animals (n=3). Germline stem cell (GSC),
410 spermatogonia (SG), spermatocyte (SC). (C) Spatial distribution of LD (grey histogram)
411 and GFP expression (green line) in testes from *bmm-GFP* animals as a function of
412 distance from the hub (n=3). (D,E) LD near the apical region of the testis in bmm^{rev} (D)
413 or bmm^{1} (E) animals. (F) LD further away from the apical tip in bmm^{1} animals. (D–F)
414 Scale bars=50 μm. (G) Histogram representing testis LD size distribution in bmm^{rev}
415 (grey) and bmm^{1} (orange). (H) Apical tip of the testes is at the left of the graph;
416 individual dots represent a single LD and its relative position to the hub marked by an
417 asterisk. Cumulative frequency distribution of the distance between LDs and the apical
418 tip of the testes are drawn as solid lines. See also Supplemental Figure 2 and 3.
419

420 **Figure 3 – *bmm* regulates germline lipid droplets in a cell-autonomous manner.**
421 (A–B) Single confocal slices through a representative testis isolated from an individual
422 carrying clones induced using the FLP-FRT system at 3 days post-clone induction.
423 Clones are homozygous for an allele that encodes a functional *bmm* protein product
424 (*bmm*^{rev}; A–A''') or a loss-of-function *bmm* allele (*bmm*^{1}, B–B'''). GFP negative areas
425 mark homozygous clones in panel A and B; the boxed areas in A, A'' and B, B'' are
426 shown in A', A''' and B', B''', respectively. In homozygous *bmm*^{rev} spermatocyte clones
427 we detected no LD using neutral lipid dye BODIPY (A'' and A'''). In contrast,
428 spermatocyte clones homozygous for *bmm*^{1} have detectable LD (B'' and B''', arrows).
429 Scale bars=50 μm in A,A'' and B,B''; scale bars=10 μm in A',A''' and B',B'''. (C) Number
430 of testis LD in *bmm*^{rev} (grey) or *bmm*^{1} (orange) in FLP-FRT clones 3 days post-clone
431 induction; dots represent measurements from a single clone. The number of cells in
432 each cyst (CC) counted is indicated. There were significantly more LD in *bmm*^{1}
433 spermatocyte (SC) clones (p = 0.026; Welch two-sample t-test) but not at other stages
434 of development.
435
436 **Figure 4 – A cell-autonomous role for *bmm* in regulating spermatogenesis.** Testes
437 isolated from *bmm*^{rev} (A) and *bmm*^{1} (A') animals raised at 25°C stained with phalloidin.
438 Scale bars=100 μm. (B) Testis size in *bmm*^{1} and *bmm*^{rev} animals raised at 25°C. (C)
439 Spermatid bundle number in *bmm*^{1} and *bmm*^{rev} testes from animals reared at 25°C.
440 (D,E) Representative images of *bmm*^{rev} (D) or *bmm*^{1} (E) testes stained with DAPI and
441 anti-Vasa antibody. Arrows indicate germline stem cells (GSC). Scale bar=50 μm. The
442 hub is marked by an asterisk in all images. (F) GSC number in *bmm*^{1} and *bmm*^{rev}

443 testes. (G) Proportion of GSCs that were either *bmm*^{1} or *bmm*^{rev} clones at 3 and 14
444 days post-clone induction. (H) Representative images of *bmm*^{rev} (H) and *bmm*^{1} (H')
445 testes carrying *bam-GFP*; data quantified in Figure S4J. Arrows indicate regions with
446 high Bam-GFP. Scale bars=50 μm. (I) Representative images of *bmm*^{rev} (I) or *bmm*^{1}
447 (I',I'') testes stained with anti-Vasa antibody. Arrows indicate Vasa-positive cysts in
448 *bmm*^{1} testis. Panel I'' is magnified from the boxed region in I'. (I,I') Scale bars=100 μm;
449 (I'') scale bar=50 μm. (J) Maximum projection of *bmm*^{rev} (J) or *bmm*^{1} (J') testes stained
450 with anti-Boule antibody (green) and DAPI (blue). Scale bars=100 μm. Number of *bmm*^{1}
451 and *bmm*^{rev} spermatocyte clones (K) or post-meiotic clones (L) at 3- and 14-days post-
452 clone induction. See also Supplemental Figure 4.
453
454 **Figure 5 – Loss of *bmm* disrupts triglyceride homeostasis and leads to**
455 **spermatogenic defects.** (A) Hierarchical clustering of lipid species detected in *bmm*^{rev}
456 and *bmm*^{1} animals. (B) Histograms showing the proportion of species in each lipid class
457 with different levels between *bmm*^{1} and *bmm*^{rev}. Numbers on histograms indicate the
458 number of species with differences in abundance. (C) Volcano plot showing fold change
459 in abundance of triglycerides (green; 97 species) and non-triglyceride lipids (grey; 186
460 species) in our dataset. (D) Arrows indicate testis LD stained with LipidTox Red in
461 *bmm*^{rev} (D), *bmm*^{1} (D'), or *mdy*$^{QX25/k03902}$; *bmm*^{1} (D'') animals. (E) Whole testes isolated
462 from *bmm*^{rev} (E), *bmm*^{1} (E'), or *mdy*$^{QX25/k03902}$;*bmm*^{1} (E'') animals stained with anti-Vasa
463 antibody (red) and DAPI (blue). Arrowheads indicate spermatid bundles. Scale
464 bars=100 μm. (F) Testis size in *bmm*^{rev}, *bmm*^{1}, and *mdy*$^{QX25/k03902}$;*bmm*^{1} animals.
465 Spermatid bundles (G) and number of germline stem cells (H) in *bmm*^{rev}, *bmm*^{1}, and

466 *mdy*$^{QX25/k03902}$;*bmm*^{1} animals. (I) Testis size in animals with germline-specific *mdy*

467 knockdown (*nos-GAL4>mdy RNAi*; *bmm*^{1}) compared with controls (*nos-GAL4*>+; *bmm*^{1}

468 and +>*mdy RNAi*; *bmm*^{1}). See also Supplemental Figure 5.

469

470 **Figure 6 – Model of *bmm*-mediated lipid droplet regulation in the *Drosophila***

471 **testis.** Schematic representation summarizing *bmm*-mediated lipid droplet regulation in

472 the testis during development.

473

474 **MATERIALS AND METHODS**

475

476 ***Materials and Resource availability.*** *Drosophila* strains and their source are listed in a
477 Key Resources table. Further information and requests for resources and reagents
478 should be directed to, and will be fulfilled by, lead contact Dr. Elizabeth J. Rideout
479 (elizabeth.rideout@ubc.ca).

480

481 ***Data and Code availability.*** All raw data and results of statistical tests reported in this
482 paper are located in Supplementary files 1-4. This paper does not report original code.
483 Any additional information required to reanalyze the data reported in this paper is
484 available from the lead contact upon request.

485

486 ***Fly husbandry.*** Fly stocks were maintained at room temperature in 12:12 hour
487 light:dark cycle. Unless otherwise indicated, all flies were raised at 25°C with a density
488 of 50 larvae per 10 mL fly media. Because this project examines sperm development,
489 we used male flies in all experiments. Fly media contained 20.5 g sucrose (SU10, Snow
490 Cap), 70.9 g Dextrose (SUG8, Snow Cap), 48.5 g cornmeal (AO18006, Snow Cap),
491 30.3 g baker's yeast (NB10, Snow Cap), 4.55 g agar (DR-820-25F, SciMart), 0.5 g
492 calcium chloride dihydrate (CCL302.1, BioShop Canada), 0.5 g magnesium sulfate
493 heptahydrate (MAG511.1, BioShop Canada), 4.9 mL propionic acids (P1386, Sigma-
494 Aldrich), and 488 µL phosphoric acid (P5811, Sigma-Aldrich) per 1L of media. For diets
495 with medium- or long-chain triglyceride, 4 g of coconut oil (medium chain triglyceride) or
496 olive oil (long chain triglyceride) was added per 100 mL of media described above prior

497 to cooling. Males were collected and dissected within 24 hours of eclosion unless
498 otherwise indicated. Fixations were performed at room temperature with 4%
499 paraformaldehyde (CA11021-168, VWR) in PBS for 20 minutes on a rotating platform
500 followed by washing in PBS twice before staining. Fly strains used in our study are
501 listed in a Key Resources table.
502
503 ***Testis cell stage classification and measurements*.** Cells at an early stage of
504 development (stem cells and early-stage somatic and germline cells) were located in
505 the apical region of the testis, and were identified by their small and dense nuclei[120].
506 GSCs were defined as Vasa-positive cells in direct contact with the hub; proliferating
507 GSCs were identified as Vasa-positive cells in direct contact with the hub that were also
508 phospho-H3 positive. Cells in the testis region occupied by primary spermatocytes were
509 identified by their large cell size and decondensed chromosome staining occupying
510 three nuclear domains [120]. Spermatid bundles were identified by their condensed and
511 needle-shaped nuclei, which roughly corresponds to nuclei with protamine-based
512 chromatin [121]. Hub size was measured by quantifying FasIII-positive area of the
513 testis. Testis size was measured by quantifying the length of a line drawn down the
514 middle of a testis image; starting from the apical tip of the testis and ending where the
515 testis meets the seminal vesicle.
516
517 ***FLP-FRT clone induction.*** Adult males were collected at 3-5 days post-eclosion and
518 heat-shocked three times at 37°C for 30 min followed by a 10 min rest period at room

519 temperature between heat shocks. After heat-shock, the flies were incubated at room
520 temperature until dissection.
521
522 ***Immunohistochemistry.*** Fixed samples were rinsed three times with blocking solution
523 containing 0.2% bovine serum albumin (A4503, Sigma-Aldrich), 0.3% Triton-X in PBS,
524 then blocked for 1 hr on a rotating platform at room temperature. During the incubation,
525 the blocking solution was changed every 15 minutes. After blocking, the sample were
526 resuspended in blocking solution with the appropriate concentration of primary antibody
527 (see Key Resources table), and incubated overnight at 4°C. Samples were rinsed three
528 times with blocking solution after removing primary antibody, and blocked for one hour
529 on a rotating platform in blocking solution. Secondary antibody was applied in blocking
530 solution and left on the rotating platform at room temperature for 40 min. The sample
531 was rinsed with blocking solution three more times, and washed four times for 15 min
532 per wash in blocking solution. Testis samples were resuspended in Vectashield
533 mounting media with DAPI (H-1200-10, Vector Laboratory) or SlowFade Diamond
534 mounting media (S36972, Thermo Fisher Scientific) prior to mounting.
535
536 ***Lipid droplet staining.*** Fixed testes were briefly permeabilized with 0.1% Triton-X in
537 PBS for 5 min prior to applying phalloidin. For BODIPY (4,4-Difluoro-1,3,5,7,8-
538 Pentamethyl-4-Bora-3a,4a-Diaza-*s*-Indacene) staining, samples were suspended in
539 PBS containing 10 µg/mL DAPI (2879083-5mg, PeproTech), 1:500 BODIPY 495/503
540 (Thermo Fisher Scientific D3922), and 1:1000 phalloidin iFluor647 (ab176759, Abcam)
541 or 1:40 phalloidin TexasRed (T7471, Thermo Fisher Scientific). For staining with

542 LipidTox Red, samples were suspended in PBS containing 10 μg/mL DAPI (2879083-
543 5mg, PeproTech), 1:200 LipidTox Red (H34476, Thermo Fisher Scientific), and 1:1000
544 phalloidin iFluor647 (ab176759, Abcam). For staining free sterols, samples were
545 prepared as for BODIPY staining with 50 μg/mL filipin in place of BODIPY for 30 min.
546 Samples were incubated on a rotating platform for 40 minutes at room temperature.
547 After incubation, samples were washed twice with PBS, then resuspended in SlowFade
548 Diamond mounting media (Thermo Fisher Scientific S36972) prior to mounting.
549
550 ***Image acquisition and processing.*** All images were acquired on a Leica SP5 confocal
551 microscope system with 20X or 40X objectives and quantified with Fiji image analysis
552 software[122].
553
554 ***Drosophila lipidomics.*** *Drosophila* extracts were prepared following the previously
555 reported protocol[123]. Briefly, 10 *Drosophila* males (~10 mg) were weighed, 300 μL of
556 ice-cold methanol/water mixture (9:1, v:v) was added to these males, and the samples
557 were homogenized with glass beads using a bead beater (mini-beadbeater-16,
558 BioSpec, Bartlesville, Ok, USA). Sample weight was used for sample normalization. Fly
559 lysate was kept at -20°C for 4 hours for protein precipitation. Then, 900 μL of methyl
560 tert-butyl ether was added and the solution was shaken for 5 min to extract lipids. To
561 induce phase separation 285 μL of water was added, followed by centrifugation. The
562 upper layer was separated, dried, and reconstituted in isopropanol/acetonitrile (1:1, v:v)
563 for liquid chromatography-mass spectrometry (LC-MS) analysis. The volume of
564 reconstitution solution was proportional to sample weight for normalization. Quality

565 control (QC) samples were prepared by pooling 20 μL aliquot from each sample. The
566 method blank sample was prepared using an identical workflow but without adding
567 *Drosophila*.
568 *Drosophila* extracts were analyzed on an UHR-QqTOF (Ultra-High Resolution
569 Qq-Time-Of-Flight) mass spectrometry Impact II (Bruker Daltonics, Bremen, Germany)
570 interfaced with an Agilent 1290 Infinity II LC Systems (Agilent Technologies, Santa
571 Clara, CA, USA). LC separation was performed using a Waters reversed-phase (RP)
572 UPLC Acquity BEH C18 Column (1.7 μm, 1.0 mm ×100 mm, 130 Å) (Milford, MA, USA)
573 maintained at 30°C. For positive ion mode, the mobile phase A was 60% acetonitrile in
574 water and the mobile phase B was 90% isopropanol in acetonitrile, both containing 5
575 mM ammonium formate (pH = 4.8, adjusted by formic acid). For negative ion mode, the
576 mobile phase A was 60% acetonitrile in water and the mobile phase B was 90%
577 isopropanol in acetonitrile, both containing 5 mM NH_4FA (pH = 9.8, adjusted by
578 ammonium hydroxide). The LC gradient for positive and negative ion modes was set as
579 follows: 0 min, 5% B; 8 min, 40% B; 14 min, 70% B; 20 min, 95% B; 23 min, 95% B; 24
580 min, 5% B; 33 min, 5% B. The flow rate was 0.1 mL/min. The injection volume was
581 optimized to 2 μL in positive mode and 5 μL in negative mode using QC sample. The
582 ESI source conditions were set as follows: dry gas temperature, 220 °C; dry gas flow, 7
583 L/min; nebulizer gas pressure, 1.6 bar; capillary voltage, 4500 V for positive mode and
584 3000 V for negative mode. The MS1 analysis was conducted using following
585 parameters: mass range, 70-1000 m/z; spectrum type: centroid, calculated using
586 maximum intensity; absolute intensity threshold: 250. Data-dependent MS/MS analysis
587 parameters: collision energy: 16-30 eV; cycle time, 3 s; spectra rate: 4 Hz when

588 intensity < 10^4 and 12 Hz when intensity > 10^5, linearly increased from 10^4 to 10^5.
589 External calibration was applied using sodium formate to ensure the m/z accuracy
590 before sample analysis.
591 The raw LC-MS data were processed using MS-DIAL (ver. 4.38)[124]. The
592 detailed MS-DIAL parameters are: MS1 tolerance, 0.01 Da; MS/MS tolerance, 0.05;
593 mass slice width, 0.05 Da; smoothing method, linear weighted moving average;
594 smoothing level, 3 scans; minimum peak width, 5 scans. Lipid features with high
595 quantitative confidence were selected by the following criteria: retention time was within
596 the gradient elution time (< 23 min); average intensity in QC samples is larger than 5-
597 fold of the intensity in method blank sample. Lipid identification was performed by
598 matching experimental precursor m/z, isotopic ratio and MS/MS spectrum against the
599 LipidBlast libraries embedded in MS-DIAL. To improve the quantification accuracy, the
600 measured MS signal intensities were corrected using serial diluted QC samples
601 following the reported workflow[125].
602
603 **Quantification and statistical analysis.** All microscopy images were quantified using
604 Fiji software[122]. For lipid droplet counts, a single optical slice through the middle of
605 the testis containing the hub was used with the exception of FLP-FRT experiment where
606 all lipid droplets within a GFP-negative cyst were counted (Figure 2I). All statistical
607 analyses were done using R (obtained from https://cran.r-project.org). With exception of
608 data concerning spatial distribution, and lipidomic data, Shapiro-Wilk test (via
609 *shapiro.test* in base R) was used to assess normality of distribution prior to testing for
610 significance. Kruskal-Wallis rank sum test (from the R package *coin*) and Dunn's test

611 (from the R package *dunn.test*) were used in place of Welch two-sample t-test and
612 Tukey's multiple comparison test when the assumption of normality was not met. For
613 testing differences in variance between two populations, F-test (via *var.test* in base R)
614 was used. For testing differences in spatial distribution, two-sample Kolmogorov-
615 Smirnov test (via *ks.test* in base R) was used. All *p*-values are indicated in figures;
616 extremely small *p*-values are listed as $p<2.2 \times 10^{-16}$.
617

618 **RESOURCE TABLE**

REAGENT or RESOURCE	SOURCE	RESOURCE #
Antibodies		
Anti-Vasa (1:200)	Gift from Dr. R. Lehman, MIT	
Anti-Eya (1:50)	Developmental Studies Hybridoma Bank (DSHB)	eya10H6
Anti-zfh1 (1:1000)	Gift from Dr. J. Skeath, WUSTL	
Anti-boule (1:1000)	Gift from Dr. S. Wasserman, UCSD	
Anti-phospho-histone H3 (1:1000)	Millipore Sigma	05-1354
Experimental models: *Drosophila melanogaster*		
w^{1118}	Bloomington *Drosophila* stock center	3605
CantonS	Bloomington *Drosophila* stock center	64349
OregonR	Bloomington *Drosophila* stock center	25211
bmm^{1}	Gift from Dr. R. Kühnlein	
bmm^{rev}	Gift from Dr. R. Kühnlein	
mdy[Qx25], cn[1], bw[1]/CyO, l(2)DTS513[1]	Bloomington *Drosophila* stock center	5095
y[1],w[67c23];P{lacW}Cse1[k03802],mdy[k03902]/CyO	Bloomington *Drosophila* stock center	10536
w[1118];P{GD1749}v6367 (UAS-mdy-RNAi)	Vienna *Drosophila* resource center	6367

REAGENT or RESOURCE	SOURCE	RESOURCE #
nos-GAL4::VP16	Bloomington *Drosophila* stock center	7303
Tj-GAL4	Gift from Dr. D. Godt, University of Toronto	
c587-GAL4	Bloomington *Drosophila* stock center	67747
Bam-GFP	[40]	
bmm-GFP	Gift from Dr. K. Kamei[57]	
GFP-LD	Gift from Dr. M. Welte[36]	
P{neoFRT}82B, bmm[1]	This study	
P{neoFRT}82B, bmm[rev]	This study	
bam-GFP, bmm[1]	This study	
bam-GFP, bmm[rev]	This study	
Software and algorithms		
Fiji	https://imagej.net/software/fiji/	
R	https://cran.r-project.org	

619

620 **SUPPLEMENTAL TABLE AND FILES**

621 **Supplemental table 1** – Table showing identified lipid species from untargeted
622 lipidomic analysis.

623 **Supplementary file 1** – Raw data and statistical outputs from Figure 1.

624 **Supplementary file 2** – Raw data and statistical outputs from Figure 2, Supplemental
625 figure 2, and Supplemental figure 3.

626 **Supplementary file 3** – Raw data and statistical outputs from Figure 3 and
627 Supplemental figure 4.
628 **Supplementary file 4** – Raw data and statistical outputs from Figure 4 and
629 Supplemental figure 5.
630
631 **SUPPLEMENTAL FIGURE LEGENDS**
632 **Supplemental Figure 1 related to Figure 1 – Cholesterol is absent from testis lipid**
633 **droplets.** (A) Testes stained with BODIPY (A) to detect neutral lipids and Filipin III (A')
634 to detect free cholesterol. Scale bars=50 μm.
635
636 **Supplemental Figure 2 related to Figure 2 – Expression of *brummer* and selected**
637 **lipid metabolic genes during spermatogenesis in germline and somatic lineages.**
638 (A) Pseudotime trajectory of germline (black line) based on single-cell RNA sequencing
639 data [78]. Individual cells are labeled according to the annotation within the data set. (B)
640 Pseudotime trajectory of the somatic cells (black line) based on publicly available
641 single-cell RNA sequencing data [78]. Individual cells are labeled according to the
642 annotation within the data set. Only one trajectory (branch b) is marked and used for
643 panel D. (C) Rolling average of normalized transcript counts in the germline along the
644 trajectory shown in panel A are plotted as a black line on the upper panel. Composition
645 of cell types mapped on to the trajectory at each time point is shown at the bottom of
646 panel B. (D) Rolling average of normalized transcript counts in somatic cells plotted as a
647 black line along the trajectory shown in C (upper panel). Composition of cell types
648 mapped on to the trajectory at each time point is shown at the bottom of panel D.

649

650 **Supplemental Figure 3 related to Figure 2 – *brummer* regulates lipid droplets in**
651 **both germline and somatic cells of the testis.** (A-D) Representative images of
652 *bmm*^{rev} (A and B) and *bmm*^{1} (C and D) testes with somatic over-expression of *GFP-LD*
653 (*Tj-GAL4>UAS-GFP-LD*). Panel F and H contain magnified images of the area indicated
654 by the boxes in panel A and C, respectively. In *bmm*^{rev} testes, LD were restricted to a
655 region near the apical tip (A) of the testis in both somatic (B–B''' arrows) and germline
656 cells (B–B''' arrowheads). In *bmm*^{1} testes, LD were present in both somatic (C–D
657 arrows) and germline cells (C–D arrowheads), near the apical tip of the testis in a region
658 corresponding to early-stage germ cells and in the region corresponding to
659 spermatocytes. (A,C) Scale bars=50 μm; (B,D) scale bars=20 μm.

660

661 **Supplemental Figure 4 related to Figure 4 – Additional characterization of testis**
662 **development and spermatogenesis in animals lacking *bmm*.** (A) Testis size was
663 smaller in *bmm*^{1} mutant animals compared with *bmm*^{rev} controls at <24 hr post-eclosion
664 when raised at 29°C (A; Welch two-sample t-test). (B) The number of spermatid bundles
665 was significantly lower in *bmm*^{1} mutant animals compared with *bmm*^{rev} controls at <24
666 hr post-eclosion when raised at 29°C (Kruskal-Wallis rank sum test). (C) Testis size was
667 significantly smaller in *bmm*^{1} mutant males compared with *bmm*^{rev} control males at 14-
668 days post-eclosion (Welch two-sample t-test). (D) While the median number of
669 spermatid bundles was not significantly different between *bmm*^{1} mutant males and
670 *bmm*^{rev} control males at 14 days post-eclosion (Welch two-sample t-test), 8/27 *bmm*^{1}
671 testis had no spermatid bundles, a phenotype absent in age-matched *bmm*^{rev} males

672 (0/22) (p=0.0163, Pearson's Chi-squared test), suggesting a subtle defect is present.
673 (E) Food supplemented with 4% medium chain triglyceride (MCT), but not long chain
674 triglyceride (LCT), significantly increased testis length in *bmm*^{1} animals but had no effect
675 on this phenotype in *bmm*^{rev} control animals (one-way ANOVA with Tukey multiple
676 comparison test). (F) Food supplemented with 4% medium chain triglyceride
677 significantly increased the number of spermatid bundles in *bmm*^{1} testes but had no
678 effect on this phenotype in *bmm*^{rev} control animals (one-way ANOVA with Tukey
679 multiple comparison test). (G) Representative images of *bmm*^{rev} (G–G') or *bmm*^{1} (G''–
680 G''') testes stained for Fas3 (G and G'') and Vas (G' and G'''). Scale bars=25 μm. (H)
681 Quantification of hub area in *bmm*^{rev} or *bmm*^{1} testes showed a significantly larger hub
682 size in *bmm*^{1} testes (Welch two-sample t-test). (I) The number of germline stem cells
683 (GSC) undergoing mitosis (phospho-histone H3^{+} GSC/total GSC) was not significantly
684 different between *bmm*^{1} and *bmm*^{rev} testes (Kruskal-Wallis rank sum test). (J) The
685 distance between the hub and the first Bam-GFP positive cyst (Figure 3H) was
686 significantly higher in *bmm*^{1} testes than in *bmm*^{rev} testes (Welch two-sample t-test). (K)
687 All *bmm*^{rev} testes and most *bmm*^{1} testes contained spermatids when raised at 25°C;
688 however, the most advanced stage of spermatogenesis observed in the majority of
689 *bmm*^{1} testes isolated from animals reared at 29°C was the spermatocyte stage. (L)
690 Testes isolated from *bmm*^{1} animals showed a significantly smaller Boule-positive area
691 than control testes (Welch two-sample t-test). (M) Testes isolated from *bmm*^{1} animals
692 contain fewer individualization complexes than *bmm*^{rev} control testes (Kruskal-Wallis
693 rank sum test). (N) Fewer waste bags were present in testes isolated from *bmm*^{1}
694 animals compared with *bmm*^{rev} control testes (Kruskal-Wallis rank sum test). (O)

695 Proportion of Zfh-1 positive clones that were homozygous for either *bmm*^{1} or *bmm*^{rev} at
696 3 and 14 days post-clone induction (Kruskal-Wallis rank sum test). (P) The location of
697 Zfh-1 positive clones homozygous for either *bmm*^{1} or *bmm*^{rev} at 3 and 14 days post-
698 clone induction measured as the distance from the center of the hub. Clones
699 homozygous for *bmm*^{1} locate significantly closer to the hub than the wildtype clones
700 (Kruskal-Wallis rank sum test).
701
702 **Supplemental Figure 5 related to Figure 5 – Lipidomic analysis of animals lacking**
703 ***bmm*.** (A) Higher fold-changes of triglycerides in *bmm*^{1} animals were associated with
704 less saturation in the acyl-groups (Kendall's rank correlation test). (B) Higher fold-
705 changes of triglycerides in *bmm*^{1} animals were associated with higher number of
706 carbons in the acyl-groups (Kendall's rank correlation test). Each dot represents a single
707 triglyceride species for panel B and C. (C) Volcano plot of identified lipids;
708 monoglycerides shown in blue and diglycerides shown in orange. Many monoglycerides
709 and diglycerides show increase in fold-change in *bmm*^{1} males. (D) The number of
710 carbon and the degree of saturation of monoglycerides (MAG) and diglycerides (DAG)
711 with significant changes in abundance between *bmm*^{1} and *bmm*^{rev} males. (E) Volcano
712 plot of identified lipids; fatty acids shown in magenta and acyl-carnitine shown in green.
713 Many fatty acids show an increase in fold-change while many acyl-carnitines show a
714 decrease in fold-change in *bmm*^{1} males. (F) The number of carbon and the degree of
715 saturation of fatty acids (FA) and acyl-carnitines (ACar) with significant changes in
716 abundance between *bmm*^{1} and *bmm*^{rev} males. (G) Volcano plot of identified lipids;
717 membrane lipids shown in yellow. (H) The number of carbon and the degree of

718 saturation of membrane lipids with significant changes in abundance between *bmm*^{1}

719 and *bmm*^{rev} males. For panel G and H, PC: phosphatidylcholine; PE:

720 phosphatidylethanolamine; PI: phosphatidylinositol; LPC: lysophosphatidylcholine; LPE:

721 lysophosphatidylethanolamine; SM: sphingomyelin; PG: phosphatidylglycerol. (I) Loss

722 of *mdy* function rescued the elevated number of LD in *bmm*^{1} testes to control levels

723 (one-way ANOVA with Tukey multiple comparison test). (J) Germline-specific loss of

724 *mdy* in *bmm*^{1} animals did not reduce GSC numbers, but the variance in GSC numbers

725 was significantly rescued (*nos-GAL4*>+; *bmm*^{1} vs *nos-GAL4*>*mdy RNAi*; *bmm*^{1}: p=4.5 ×

726 10^{-5}; +>*mdy RNAi*; *bmm*^{1} vs *nos-GAL4*>*mdy RNAi*; *bmm*^{1}: p=0.0082 by F-test).

727
728

729 **REFERENCES**
730

731 1. Brill JA, Yildirim S, Fabian L. Phosphoinositide signaling in sperm development. Semin Cell
732 Dev Biol. 2016;59: 2–9. doi:10.1016/j.semcdb.2016.06.010

733 2. Keber R, Rozman D, Horvat S. Sterols in spermatogenesis and sperm maturation. J Lipid Res.
734 2013;54: 20–33. doi:10.1194/jlr.R032326

735 3. Rato L, Alves MG, Socorro S, Duarte AI, Cavaco JE, Oliveira PF. Metabolic regulation is
736 important for spermatogenesis. Nat Rev Urol. 2012;9: 330–338.
737 doi:10.1038/nrurol.2012.77

738 4. Wang C, Huang X. Lipid metabolism and Drosophila sperm development. Sci China Life Sci.
739 2012;55: 35–40. doi:10.1007/s11427-012-4274-2

740 5. de Cuevas M, Matunis EL. The stem cell niche: lessons from the Drosophila testis. Dev Camb
741 Engl. 2011;138: 2861–2869. doi:10.1242/dev.056242

742 6. Demarco RS, Eikenes ÅH, Haglund K, Jones DL. Investigating Spermatogenesis in Drosophila
743 melanogaster. Methods San Diego Calif. 2014;68: 218–227.
744 doi:10.1016/j.ymeth.2014.04.020

745 7. Fabian L, Brill JA. Drosophila spermiogenesis: Big things come from little packages.
746 Spermatogenesis. 2012;2: 197–212. doi:10.4161/spmg.21798

747 8. Brill JA, Hime GR, Scharer-Schuksz M, Fuller MT. A phospholipid kinase regulates actin
748 organization and intercellular bridge formation during germline cytokinesis.
749 Development. 2000;127: 3855.

750 9. Giansanti MG, Bonaccorsi S, Kurek R, Farkas RM, Dimitri P, Fuller MT, et al. The Class I PITP
751 Giotto Is Required for Drosophila Cytokinesis. Curr Biol. 2006;16: 195–201.
752 doi:10.1016/j.cub.2005.12.011

753 10. Wong R, Hadjiyanni I, Wei H-C, Polevoy G, McBride R, Sem K-P, et al. PIP2 Hydrolysis and
754 Calcium Release Are Required for Cytokinesis in Drosophila Spermatocytes. Curr Biol.
755 2005;15: 1401–1406. doi:10.1016/j.cub.2005.06.060

756 11. Wong R, Fabian L, Forer A, Brill JA. Phospholipase C and myosin light chain kinase inhibition
757 define a common step in actin regulation during cytokinesis. BMC Cell Biol. 2007;8: 15.
758 doi:10.1186/1471-2121-8-15

759 12. Amoyel M, Hillion K-H, Margolis SR, Bach EA. Somatic stem cell differentiation is regulated
760 by PI3K/Tor signaling in response to local cues. Dev Camb Engl. 2016;143: 3914.
761 doi:10.1242/dev.139782

762 13. Fairchild MJ, Islam F, Tanentzapf G. Identification of genetic networks that act in the
763 somatic cells of the testis to mediate the developmental program of spermatogenesis.
764 PLOS Genet. 2017;13: e1007026. doi:10.1371/journal.pgen.1007026

765 14. Inaba M, Venkei ZG, Yamashita YM. The polarity protein Baz forms a platform for the
766 centrosome orientation during asymmetric stem cell division in the Drosophila male
767 germline. eLife. 2015;4: e04960. doi:10.7554/eLife.04960

768 15. Krahn MP, Klopfenstein DR, Fischer N, Wodarz A. Membrane Targeting of Bazooka/PAR-3 Is
769 Mediated by Direct Binding to Phosphoinositide Lipids. Curr Biol. 2010;20: 636–642.
770 doi:10.1016/j.cub.2010.01.065

771 16. Papagiannouli F, Berry CW, Fuller MT. The Dlg Module and Clathrin-Mediated Endocytosis
772 Regulate EGFR Signaling and Cyst Cell-Germline Coordination in the Drosophila Testis.
773 Stem Cell Rep. 2019;12: 1024–1040. doi:10.1016/j.stemcr.2019.03.008

774 17. Ueishi S, Shimizu H, Inoue YH. Male Germline Stem Cell Division and Spermatocyte Growth
775 Require Insulin Signaling in Drosophila. Cell Struct Funct. 2009;34: 61–69.
776 doi:10.1247/csf.08042

777 18. Phan VH, Herr DR, Panton D, Fyrst H, Saba JD, Harris GL. Disruption of Sphingolipid
778 Metabolism Elicits Apoptosis-Associated Reproductive Defects in Drosophila. Dev Biol.
779 2007;309: 329–341. doi:10.1016/j.ydbio.2007.07.021

780 19. Steinhauer J, Gijón MA, Riekhof WR, Voelker DR, Murphy RC, Treisman JE. Drosophila
781 Lysophospholipid Acyltransferases Are Specifically Required for Germ Cell Development.
782 Mol Biol Cell. 2009;20: 5224–5235. doi:10.1091/mbc.e09-05-0382

783 20. Szafer-Glusman E, Giansanti MG, Nishihama R, Bolival B, Pringle J, Gatti M, et al. A Role for
784 Very-Long-Chain Fatty Acids in Furrow Ingression during Cytokinesis in Drosophila
785 Spermatocytes. Curr Biol. 2008;18: 1426–1431. doi:10.1016/j.cub.2008.08.061

786 21. Ben-David G, Miller E, Steinhauer J. Drosophila spermatid individualization is sensitive to
787 temperature and fatty acid metabolism. Spermatogenesis. 2015;5.
788 doi:10.1080/21565562.2015.1006089

789 22. Jung A, Hollmann M, Schafer MA. The fatty acid elongase NOA is necessary for viability and
790 has a somatic role in Drosophila sperm development. J Cell Sci. 2007;120: 2924–2934.
791 doi:10.1242/jcs.006551

792 23. Rabionet M, Bayerle A, Jennemann R, Heid H, Fuchser J, Marsching C, et al. Male meiotic
793 cytokinesis requires ceramide synthase 3-dependent sphingolipids with unique
794 membrane anchors. Hum Mol Genet. 2015;24: 4792–4808. doi:10.1093/hmg/ddv204

795 24. Santiago Valtierra FX, Peñalva DA, Luquez JM, Furland NE, Vásquez C, Reyes JG, et al. Elovl4
796 and Fa2h expression during rat spermatogenesis: a link to the very-long-chain PUFAs

797 typical of germ cell sphingolipids. J Lipid Res. 2018;59: 1175–1189.
798 doi:10.1194/jlr.M081885

799 25. Zadravec D, Tvrdik P, Guillou H, Haslam R, Kobayashi T, Napier JA, et al. ELOVL2 controls the
800 level of n-6 28:5 and 30:5 fatty acids in testis, a prerequisite for male fertility and sperm
801 maturation in mice. J Lipid Res. 2011;52: 245–255. doi:10.1194/jlr.M011346

802 26. Walther TC, Farese RV. Lipid Droplets and Cellular Lipid Metabolism. Annu Rev Biochem.
803 2012;81: 687–714. doi:10.1146/annurev-biochem-061009-102430

804 27. Wat LW, Chao C, Bartlett R, Buchanan JL, Millington JW, Chih HJ, et al. A role for triglyceride
805 lipase brummer in the regulation of sex differences in Drosophila fat storage and
806 breakdown. Hassan BA, editor. PLOS Biol. 2020;18: e3000595.
807 doi:10.1371/journal.pbio.3000595

808 28. Thiele C, Spandl J. Cell biology of lipid droplets. Curr Opin Cell Biol. 2008;20: 378–385.
809 doi:10.1016/j.ceb.2008.05.009

810 29. Bosma M. Lipid droplet dynamics in skeletal muscle. Exp Cell Res. 2016;340: 180–186.
811 doi:10.1016/j.yexcr.2015.10.023

812 30. Grönke S, Müller G, Hirsch J, Fellert S, Andreou A, Haase T, et al. Dual Lipolytic Control of
813 Body Fat Storage and Mobilization in Drosophila. PLOS Biol. 2007;5: e137.
814 doi:10.1371/journal.pbio.0050137

815 31. Rambold AS, Cohen S, Lippincott-Schwartz J. Fatty Acid Trafficking in Starved Cells:
816 Regulation by Lipid Droplet Lipolysis, Autophagy, and Mitochondrial Fusion Dynamics.
817 Dev Cell. 2015;32: 678–692. doi:10.1016/j.devcel.2015.01.029

818 32. Dichlberger A, Schlager S, Maaninka K, Schneider WJ, Kovanen PT. Adipose triglyceride
819 lipase regulates eicosanoid production in activated human mast cells. J Lipid Res.
820 2014;55: 2471–2478. doi:10.1194/jlr.M048553

821 33. Mitsche MA, Hobbs HH, Cohen JC. Patatin-like phospholipase domain–containing protein 3
822 promotes transfers of essential fatty acids from triglycerides to phospholipids in hepatic
823 lipid droplets. J Biol Chem. 2018;293: 6958–6968. doi:10.1074/jbc.RA118.002333

824 34. Rajakumari S, Rajasekharan R, Daum G. Triacylglycerol lipolysis is linked to sphingolipid and
825 phospholipid metabolism of the yeast Saccharomyces cerevisiae☆. Biochim Biophys Acta
826 BBA - Mol Cell Biol Lipids. 2010;1801: 1314–1322. doi:10.1016/j.bbalip.2010.08.004

827 35. Schlager S, Goeritzer M, Jandl K, Frei R, Vujic N, Kolb D, et al. Adipose triglyceride lipase acts
828 on neutrophil lipid droplets to regulate substrate availability for lipid mediator synthesis.
829 J Leukoc Biol. 2015;98: 837–850. doi:10.1189/jlb.3A0515-206R

830 36. Zanghellini J, Natter K, Jungreuthmayer C, Thalhammer A, Kurat CF, Gogg-Fassolter G, et al.
831 Quantitative modeling of triacylglycerol homeostasis in yeast - metabolic requirement for
832 lipolysis to promote membrane lipid synthesis and cellular growth: Triacylglycerol
833 mobilization in yeast. FEBS J. 2008;275: 5552–5563. doi:10.1111/j.1742-
834 4658.2008.06681.x

835 37. Bailey AP, Koster G, Guillermier C, Hirst EMA, MacRae JI, Lechene CP, et al. Antioxidant Role
836 for Lipid Droplets in a Stem Cell Niche of Drosophila. Cell. 2015;163: 340–353.
837 doi:10.1016/j.cell.2015.09.020

838 38. Liu L, MacKenzie KR, Putluri N, Maletić-Savatić M, Bellen HJ. The Glia-Neuron Lactate
839 Shuttle and Elevated ROS Promote Lipid Synthesis in Neurons and Lipid Droplet
840 Accumulation in Glia via APOE/D. Cell Metab. 2017;26: 719-737.e6.
841 doi:10.1016/j.cmet.2017.08.024

842 39. Nguyen TB, Louie SM, Daniele JR, Tran Q, Dillin A, Zoncu R, et al. DGAT1-Dependent Lipid
843 Droplet Biogenesis Protects Mitochondrial Function during Starvation-Induced
844 Autophagy. Dev Cell. 2017;42: 9-21.e5. doi:10.1016/j.devcel.2017.06.003

845 40. Henne M. And three's a party: lysosomes, lipid droplets, and the ER in lipid trafficking and
846 cell homeostasis. Curr Opin Cell Biol. 2019;59: 40–49. doi:10.1016/j.ceb.2019.02.011

847 41. Welte MA. Expanding Roles for Lipid Droplets. Curr Biol. 2015;25: R470–R481.
848 doi:10.1016/j.cub.2015.04.004

849 42. Casado ME, Pastor O, Mariscal P, Canfrán-Duque A, Martínez-Botas J, Kraemer FB, et al.
850 Hormone-sensitive lipase deficiency disturbs the fatty acid composition of mouse testis.
851 Prostaglandins Leukot Essent Fatty Acids. 2013;88: 227–233.
852 doi:10.1016/j.plefa.2012.12.005

853 43. El-Shehawi AM, El-Shazly S, Ahmed M, Alkafafy M, Sayed S, Farouk S, et al. Transcriptome
854 Analysis of Testis from HFD-Induced Obese Rats (Rattus norvigicus) Indicated
855 Predisposition for Male Infertility. Int J Mol Sci. 2020;21: 6493.
856 doi:10.3390/ijms21186493

857 44. Wang W, Wei S, Li L, Su X, Du C, Li F, et al. Proteomic analysis of murine testes lipid
858 droplets. Sci Rep. 2015;5: 12070. doi:10.1038/srep12070

859 45. Bajpai M, Gupta G, Setty BS. Changes in carbohydrate metabolism of testicular germ cells
860 during meiosis in the rat. Eur J Endocrinol. 1998;138: 322–327.

861 46. Kerr JB, Kretser DMD. CYCLIC VARIATIONS IN SERTOLI CELL LIPID CONTENT THROUGHOUT
862 THE SPERMATOGENIC CYCLE IN THE RAT. Reproduction. 1975;43: 1–8.
863 doi:10.1530/jrf.0.0430001

864 47. Mori H, Christensen AK. Morphometric analysis of Leydig cells in the normal rat testis. J Cell
865 Biol. 1980;84: 340–354. doi:10.1083/jcb.84.2.340

866 48. Paniagua R, Rodríguez MC, Nistal M, Fraile B, Amat P. Changes in the lipid inclusion/Sertoli
867 cell cytoplasm area ratio during the cycle of the human seminiferous epithelium.
868 Reproduction. 1987;80: 335–341. doi:10.1530/jrf.0.0800335

869 49. Demarco RS, Uyemura BS, D'Alterio C, Jones DL. Mitochondrial fusion regulates lipid
870 homeostasis and stem cell maintenance in the Drosophila testis. Nat Cell Biol. 2019;21:
871 710–720. doi:10.1038/s41556-019-0332-3

872 50. Chen M, Wang H, Li X, Li N, Xu G, Meng Q. PLIN1 deficiency affects testicular gene
873 expression at the meiotic stage in the first wave of spermatogenesis. Gene. 2014;543:
874 212–219. doi:10.1016/j.gene.2014.04.021

875 51. Hermo L, Chung S, Gregory M, Smith CE, Wang SP, El-Alfy M, et al. Alterations in the testis
876 of hormone sensitive lipase-deficient mice is associated with decreased sperm counts,
877 sperm motility, and fertility. Mol Reprod Dev. 2008;75: 565–577. doi:10.1002/mrd.20800

878 52. Masaki H, Kim N, Nakamura H, Kumasawa K, Kamata E, Hirano K, et al. Long-chain fatty acid
879 triglyceride (TG) metabolism disorder impairs male fertility: a study using adipose
880 triglyceride lipase deficient mice. MHR Basic Sci Reprod Med. 2017;23: 452–460.
881 doi:10.1093/molehr/gax031

882 53. Freeman DA, Ascoli M. Studies on the source of cholesterol used for steroid biosynthesis in
883 cultured Leydig tumor cells. J Biol Chem. 1982;257: 14231–14238.

884 54. Wang F, Chen Z, Ren X, Tian Y, Wang F, Liu C, et al. Hormone-sensitive lipase deficiency
885 alters gene expression and cholesterol content of mouse testis. Reproduction. 2017;153:
886 175–185. doi:10.1530/REP-16-0484

887 55. de Cuevas M, Matunis EL. The stem cell niche: lessons from the Drosophila testis.
888 Development. 2011;138: 2861–2869. doi:10.1242/dev.056242

889 56. Walther TC, Chung J, Jr RVF. Lipid Droplet Biogenesis. Annu Rev Cell Dev Biol. 2017;33: 491–
890 510. doi:10.1146/annurev-cellbio-100616-060608

891 57. Boyle M, DiNardo S. Specification, migration and assembly of the somatic cells of the
892 Drosophila gonad. Development. 1995;121: 1815–1825. doi:10.1242/dev.121.6.1815

893 58. Yu YV, Li Z, Rizzo NP, Einstein J, Welte MA. Targeting the motor regulator Klar to lipid
894 droplets. BMC Cell Biol. 2011;12: 9. doi:10.1186/1471-2121-12-9

895 59. Leatherman JL, DiNardo S. Zfh-1 Controls Somatic Stem Cell Self-Renewal in the Drosophila
896 Testis and Nonautonomously Influences Germline Stem Cell Self-Renewal. Cell Stem Cell.
897 2008;3: 44–54. doi:10.1016/j.stem.2008.05.001

898 60. Fabrizio JJ, Boyle M, DiNardo S. A somatic role for eyes absent (eya) and sine oculis (so) in
899 drosophila spermatocyte development. Dev Biol. 2003;258: 117–128.
900 doi:10.1016/S0012-1606(03)00127-1

901 61. Chen D, McKearin DM. A discrete transcriptional silencer in the bam gene determines
902 asymmetric division of the Drosophila germline stem cell. Development. 2003;130: 1159–
903 1170. doi:10.1242/dev.00325

904 62. Insco ML, Leon A, Tam CH, McKearin DM, Fuller MT. Accumulation of a differentiation
905 regulator specifies transit amplifying division number in an adult stem cell lineage. Proc
906 Natl Acad Sci U S A. 2009;106: 22311–22316. doi:10.1073/pnas.0912454106

907 63. Chen D, Wu C, Zhao S, Geng Q, Gao Y, Li X, et al. Three RNA Binding Proteins Form a
908 Complex to Promote Differentiation of Germline Stem Cell Lineage in Drosophila. PLoS
909 Genet. 2014;10. doi:10.1371/journal.pgen.1004797

910 64. Gonczy P, Matunis E, DiNardo S. bag-of-marbles and benign gonial cell neoplasm act in the
911 germline to restrict proliferation during Drosophila spermatogenesis. Development.
912 1997;124: 4361–4371.

913 65. Athenstaedt K, Daum G. YMR313c/TGL3 Encodes a Novel Triacylglycerol Lipase Located in
914 Lipid Particles of Saccharomyces cerevisiae*. J Biol Chem. 2003;278: 23317–23323.
915 doi:10.1074/jbc.M302577200

916 66. Chitraju C, Trötzmüller M, Hartler J, Wolinski H, Thallinger GG, Haemmerle G, et al. The
917 impact of genetic stress by ATGL deficiency on the lipidome of lipid droplets from murine
918 hepatocytes. J Lipid Res. 2013;54: 2185–2194. doi:10.1194/jlr.M037952

919 67. Grönke S, Mildner A, Fellert S, Tennagels N, Petry S, Müller G, et al. Brummer lipase is an
920 evolutionary conserved fat storage regulator in Drosophila. Cell Metab. 2005;1: 323–330.
921 doi:10.1016/j.cmet.2005.04.003

922 68. Haemmerle G, Lass A, Zimmermann R, Gorkiewicz G, Meyer C, Rozman J, et al. Defective
923 Lipolysis and Altered Energy Metabolism in Mice Lacking Adipose Triglyceride Lipase.
924 Science. 2006;312: 734–737. doi:10.1126/science.1123965

925 69. Haemmerle G, Moustafa T, Woelkart G, Büttner S, Schmidt A, van de Weijer T, et al. ATGL-
926 mediated fat catabolism regulates cardiac mitochondrial function via PPAR-α and PGC-1.
927 Nat Med. 2011;17: 1076–1085. doi:10.1038/nm.2439

928 70. Huijsman E, van de Par C, Economou C, van der Poel C, Lynch GS, Schoiswohl G, et al.
929 Adipose triacylglycerol lipase deletion alters whole body energy metabolism and impairs
930 exercise performance in mice. Am J Physiol-Endocrinol Metab. 2009;297: E505–E513.
931 doi:10.1152/ajpendo.00190.2009

932 71. Korbelius M, Vujic N, Sachdev V, Obrowsky S, Rainer S, Gottschalk B, et al. ATGL/CGI-58-
933 Dependent Hydrolysis of a Lipid Storage Pool in Murine Enterocytes. Cell Rep. 2019;28:
934 1923-1934.e4. doi:10.1016/j.celrep.2019.07.030

935 72. Kurat CF, Natter K, Petschnigg J, Wolinski H, Scheuringer K, Scholz H, et al. Obese Yeast:
936 Triglyceride Lipolysis Is Functionally Conserved from Mammals to Yeast *. J Biol Chem.
937 2006;281: 491–500. doi:10.1074/jbc.M508414200

938 73. Zimmermann R, Strauss JG, Haemmerle G, Schoiswohl G, Birner-Gruenberger R, Riederer M,
939 et al. Fat Mobilization in Adipose Tissue Is Promoted by Adipose Triglyceride Lipase.
940 Science. 2004;306: 1383–1386. doi:10.1126/science.1100747

941 74. Attané C, Peyot M-L, Lussier R, Poursharifi P, Zhao S, Zhang D, et al. A beta cell ATGL-
942 lipolysis/adipose tissue axis controls energy homeostasis and body weight via insulin
943 secretion in mice. Diabetologia. 2016;59: 2654–2663. doi:10.1007/s00125-016-4105-2

944 75. Lee JH, Kong J, Jang JY, Han JS, Ji Y, Lee J, et al. Lipid Droplet Protein LID-1 Mediates ATGL-1-
945 Dependent Lipolysis during Fasting in Caenorhabditis elegans. Mol Cell Biol. 2014;34:
946 4165–4176. doi:10.1128/MCB.00722-14

947 76. Tuohetahuntila M, Molenaar MR, Spee B, Brouwers JF, Houweling M, Vaandrager AB, et al.
948 ATGL and DGAT1 are involved in the turnover of newly synthesized triacylglycerols in
949 hepatic stellate cells. J Lipid Res. 2016;57: 1162–1174. doi:10.1194/jlr.M066415

950 77. Men TT, Thanh DNV, Yamaguchi M, Suzuki T, Hattori G, Arii M, et al. A *Drosophila* Model for
951 Screening Antiobesity Agents. BioMed Res Int. 2016;2016: 1–10.
952 doi:10.1155/2016/6293163

953 78. Li H, Janssens J, Waegeneer MD, Kolluru SS, Davie K, Gardeux V, et al. Fly Cell Atlas: a single-
954 cell transcriptomic atlas of the adult fruit fly. bioRxiv; 2021. p. 2021.07.04.451050.
955 doi:10.1101/2021.07.04.451050

956 79. Xu T, Rubin GM. Analysis of genetic mosaics in developing and adult Drosophila tissues.
957 Development. 1993;117: 1223–1237.

958 80. Kim N, Nakamura H, Masaki H, Kumasawa K, Hirano K, Kimura T. Effect of lipid metabolism
959 on male fertility. Biochem Biophys Res Commun. 2017;485: 686–692.
960 doi:10.1016/j.bbrc.2017.02.103

961 81. Lasko PF, Ashburner M. The product of the Drosophila gene vasa is very similar to
962 eukaryotic initiation factor-4A. Nature. 1988;335: 611–617. doi:10.1038/335611a0

963 82. Resende LPF, Boyle M, Tran D, Fellner T, Jones DL. Headcase Promotes Cell Survival and
964 Niche Maintenance in the Drosophila Testis. Bökel C, editor. PLoS ONE. 2013;8: e68026.
965 doi:10.1371/journal.pone.0068026

966 83. Kiger AA, White-Cooper H, Fuller MT. Somatic support cells restrict germline stem cell self-
967 renewal and promote differentiation. Nature. 2000;407: 750–754. doi:10.1038/35037606

968 84. Lin TY, Viswanathan S, Wood C, Wilson PG, Wolf N, Fuller MT. Coordinate developmental
969 control of the meiotic cell cycle and spermatid differentiation in Drosophila males.
970 Development. 1996;122: 1331–1341.

971 85. Eichmann TO, Kumari M, Haas JT, Farese RV, Zimmermann R, Lass A, et al. Studies on the
972 substrate and stereo/regioselectivity of adipose triglyceride lipase, hormone-sensitive
973 lipase, and diacylglycerol-O-acyltransferases. J Biol Chem. 2012;287: 41446–41457.
974 doi:10.1074/jbc.M112.400416

975 86. Schweiger M, Schreiber R, Haemmerle G, Lass A, Fledelius C, Jacobsen P, et al. Adipose
976 Triglyceride Lipase and Hormone-sensitive Lipase Are the Major Enzymes in Adipose
977 Tissue Triacylglycerol Catabolism *. J Biol Chem. 2006;281: 40236–40241.
978 doi:10.1074/jbc.M608048200

979 87. Missaglia S, Maggi L, Mora M, Gibertini S, Blasevich F, Agostoni P, et al. Late onset of
980 neutral lipid storage disease due to novel PNPLA2 mutations causing total loss of lipase
981 activity in a patient with myopathy and slight cardiac involvement. Neuromuscul Disord.
982 2017;27: 481–486. doi:10.1016/j.nmd.2017.01.011

983 88. Williams ML, Coleman RA, Placezk D, Grunfeld C. Neutral lipid storage disease: a possible
984 functional defect in phospholipid-linked triacylglycerol metabolism. Biochim Biophys Acta
985 BBA - Mol Basis Dis. 1991;1096: 162–169. doi:10.1016/0925-4439(91)90055-E

986 89. Yang L, Liang J, Lam SM, Yavuz A, Shui G, Ding M, et al. Neuronal lipolysis participates in
987 PUFA-mediated neural function and neurodegeneration. EMBO Rep. 2020;21.
988 doi:10.15252/embr.202050214

989 90. Nazario-Yepiz NO, Fernández Sobaberas J, Lyman R, Campbell MR, Shankar V, Anholt RRH,
990 et al. Physiological and metabolomic consequences of reduced expression of the
991 Drosophila brummer triglyceride Lipase. Melkani GC, editor. PLOS ONE. 2021;16:
992 e0255198. doi:10.1371/journal.pone.0255198

993 91. Giedt MS, Thomalla JM, Johnson MR, Lai ZW, Tootle TL, Welte MA. Adipose triglyceride
994 lipase promotes prostaglandin-dependent actin remodeling by regulating substrate
995 release from lipid droplets. Cell Biology; 2021 Aug. doi:10.1101/2021.08.02.454724

996 92. Beller M, Bulankina AV, Hsiao H-H, Urlaub H, Jäckle H, Kühnlein RP. PERILIPIN-Dependent
997 Control of Lipid Droplet Structure and Fat Storage in Drosophila. Cell Metab. 2010;12:
998 521–532. doi:10.1016/j.cmet.2010.10.001

999 93. Buszczak M, Lu X, Segraves WA, Chang TY, Cooley L. Mutations in the midway Gene Disrupt
1000 a Drosophila Acyl Coenzyme A: Diacylglycerol Acyltransferase. Genetics. 2002;160: 1511–
1001 1518.

1002 94. Martínez BA, Hoyle RG, Yeudall S, Granade ME, Harris TE, Castle JD, et al. Innate immune
1003 signaling in Drosophila shifts anabolic lipid metabolism from triglyceride storage to
1004 phospholipid synthesis to support immune function. PLOS Genet. 2020;16: e1009192.
1005 doi:10.1371/journal.pgen.1009192

1006 95. Freeman DA, Ascoli M. Studies on the source of cholesterol used for steroid biosynthesis in
1007 cultured Leydig tumor cells. J Biol Chem. 1982;257: 14231–14238.

1008 96. Wang F, Chen Z, Ren X, Tian Y, Wang F, Liu C, et al. Hormone-sensitive lipase deficiency
1009 alters gene expression and cholesterol content of mouse testis. Reproduction. 2017;153:
1010 175–185. doi:10.1530/REP-16-0484

1011 97. Walther TC, Farese RV. Lipid droplets and cellular lipid metabolism. Annu Rev Biochem.
1012 2012;81: 687–714. doi:10.1146/annurev-biochem-061009-102430

1013 98. Olzmann JA, Carvalho P. Dynamics and functions of lipid droplets. Nat Rev Mol Cell Biol.
1014 2019;20: 137–155. doi:10.1038/s41580-018-0085-z

1015 99. Birse RT, Choi J, Reardon K, Rodriguez J, Graham S, Diop S, et al. High-fat-diet-induced
1016 obesity and heart dysfunction are regulated by the TOR pathway in Drosophila. Cell
1017 Metab. 2010;12: 533–44. doi:10.1016/j.cmet.2010.09.014

1018 100. Molaei M, Vandehoef C, Karpac J. NF-κB Shapes Metabolic Adaptation by Attenuating
1019 Foxo-Mediated Lipolysis in Drosophila. Dev Cell. 2019;49: 802-810.e6.
1020 doi:10.1016/j.devcel.2019.04.009

1021 101. Alic N, Andrews TD, Giannakou ME, Papatheodorou I, Slack C, Hoddinott MP, et al.
1022 Genome-wide dFOXO targets and topology of the transcriptomic response to stress and
1023 insulin signalling. Mol Syst Biol. 2011;7: 502. doi:10.1038/msb.2011.36

1024 102. Junger MA, Rintelen F, Stocker H, Wasserman JD, Vegh M, Radimerski T, et al. The
1025 Drosophila forkhead transcription factor FOXO mediates the reduction in cell number
1026 associated with reduced insulin signaling. J Biol. 2003;2: 20. doi:10.1186/1475-4924-2-20

1027 103. Zinke I, Schutz CS, Katzenberger JD, Bauer M, Pankratz MJ. Nutrient control of gene
1028 expression in Drosophila: microarray analysis of starvation and sugar-dependent
1029 response. EMBO J. 2002;21: 6162–73.

1030 104. Puig O, Tjian R. Transcriptional feedback control of insulin receptor by dFOXO/FOXO1.
1031 Genes Dev. 2005;19: 2435–2446. doi:10.1101/gad.1340505

1032 105. Kang P, Chang K, Liu Y, Bouska M, Birnbaum A, Karashchuk G, et al. Drosophila Kruppel
1033 homolog 1 represses lipolysis through interaction with dFOXO. Sci Rep. 2017;7: 16369.
1034 doi:10.1038/s41598-017-16638-1

1035 106. Bartz R, Zehmer JK, Zhu M, Chen Y, Serrero G, Zhao Y, et al. Dynamic activity of lipid
1036 droplets: protein phosphorylation and GTP-mediated protein translocation. J Proteome
1037 Res. 2007;6: 3256–3265. doi:10.1021/pr070158j

1038 107. Pagnon J, Matzaris M, Stark R, Meex RCR, Macaulay SL, Brown W, et al. Identification and
1039 functional characterization of protein kinase A phosphorylation sites in the major lipolytic
1040 protein, adipose triglyceride lipase. Endocrinology. 2012;153: 4278–4289.
1041 doi:10.1210/en.2012-1127

1042 108. Narbonne P, Roy R. Caenorhabditis elegans dauers need LKB1/AMPK to ration lipid
1043 reserves and ensure long-term survival. Nature. 2009;457: 210–214.
1044 doi:10.1038/nature07536

1045 109. Ahmadian M, Abbott MJ, Tang T, Hudak CSS, Kim Y, Bruss M, et al. Desnutrin/ATGL is
1046 regulated by AMPK and is required for a brown adipose phenotype. Cell Metab. 2011;13:
1047 739–748. doi:10.1016/j.cmet.2011.05.002

1048 110. Amoyel M, Hillion K-H, Margolis SR, Bach EA. Somatic stem cell differentiation is regulated
1049 by PI3K/Tor signaling in response to local cues. Dev Camb Engl. 2016;143: 3914–3925.
1050 doi:10.1242/dev.139782

1051 111. Amoyel M, Simons BD, Bach EA. Neutral competition of stem cells is skewed by
1052 proliferative changes downstream of Hh and Hpo. EMBO J. 2014;33: 2295–2313.
1053 doi:10.15252/embj.201387500

1054 112. Ueishi S, Shimizu H, H. Inoue Y. Male Germline Stem Cell Division and Spermatocyte
1055 Growth Require Insulin Signaling in Drosophila. Cell Struct Funct. 2009;34: 61–69.
1056 doi:10.1247/csf.08042

1057 113. Hof-Michel S, Cigoja L, Huhn S, Bökel C. Innate immune signalling drives loser cell
1058 elimination during stem cell competition in the *Drosophila* testis. Developmental Biology;
1059 2020 Mar. doi:10.1101/2020.03.05.979161

1060 114. Couderc J-L, Richard G, Vachias C, Mirouse V. Drosophila LKB1 is required for the assembly
1061 of the polarized actin structure that allows spermatid individualization. White-Cooper H,
1062 editor. PLOS ONE. 2017;12: e0182279. doi:10.1371/journal.pone.0182279

1063 115. Steinhauer J, Statman B, Fagan JK, Borck J, Surabhi S, Yarikipati P, et al. Combover interacts
1064 with the axonemal component Rsp3 and is required for Drosophila sperm
1065 individualization. Dev Camb Engl. 2019;146: dev179275. doi:10.1242/dev.179275

1066 116. Tartarin P, Guibert E, Touré A, Ouiste C, Leclerc J, Sanz N, et al. Inactivation of AMPKα1
1067 induces asthenozoospermia and alters spermatozoa morphology. Endocrinology.
1068 2012;153: 3468–3481. doi:10.1210/en.2011-1911

1069 117. Martin-Hidalgo D, Hurtado de Llera A, Calle-Guisado V, Gonzalez-Fernandez L, Garcia-
1070 Marin L, Bragado MJ. AMPK Function in Mammalian Spermatozoa. Int J Mol Sci. 2018;19:
1071 3293. doi:10.3390/ijms19113293

1072 118. Pitetti J-L, Calvel P, Zimmermann C, Conne B, Papaioannou MD, Aubry F, et al. An Essential
1073 Role for Insulin and IGF1 Receptors in Regulating Sertoli Cell Proliferation, Testis Size, and
1074 FSH Action in Mice. Mol Endocrinol. 2013;27: 814–827. doi:10.1210/me.2012-1258

1075 119. Thurmond J, Goodman JL, Strelets VB, Attrill H, Gramates LS, Marygold SJ, et al. FlyBase
1076 2.0: the next generation. Nucleic Acids Res. 2018;47: D759–D765.
1077 doi:10.1093/nar/gky1003

1078 120. White-Cooper H. Spermatogenesis. In: Henderson DS, editor. Drosophila Cytogenetics
1079 Protocols. Totowa, NJ: Humana Press; 2004. pp. 45–75. doi:10.1385/1-59259-665-7:45

1080 121. Fabian L, Brill JA. Drosophila spermiogenesis. Spermatogenesis. 2012;2: 197–212.
1081 doi:10.4161/spmg.21798

1082 122. Schindelin J, Arganda-Carreras I, Frise E, Kaynig V, Longair M, Pietzsch T, et al. Fiji: an open-
1083 source platform for biological-image analysis. Nat Methods. 2012;9: 676–682.
1084 doi:10.1038/nmeth.2019

1085 123. Yu H, Villanueva N, Bittar T, Arsenault E, Labonté B, Huan T. Parallel metabolomics and
1086 lipidomics enables the comprehensive study of mouse brain regional metabolite and lipid
1087 patterns. Anal Chim Acta. 2020;1136: 168–177. doi:10.1016/j.aca.2020.09.051

1088 124. Tsugawa H, Cajka T, Kind T, Ma Y, Higgins B, Ikeda K, et al. MS-DIAL: data-independent
1089 MS/MS deconvolution for comprehensive metabolome analysis. Nat Methods. 2015;12:
1090 523–526. doi:10.1038/nmeth.3393

1091 125. Yu H, Huan T. Patterned Signal Ratio Biases in Mass Spectrometry-Based Quantitative
1092 Metabolomics. Anal Chem. 2021;93: 2254–2262. doi:10.1021/acs.analchem.0c04113

1093

1094
1095

1096

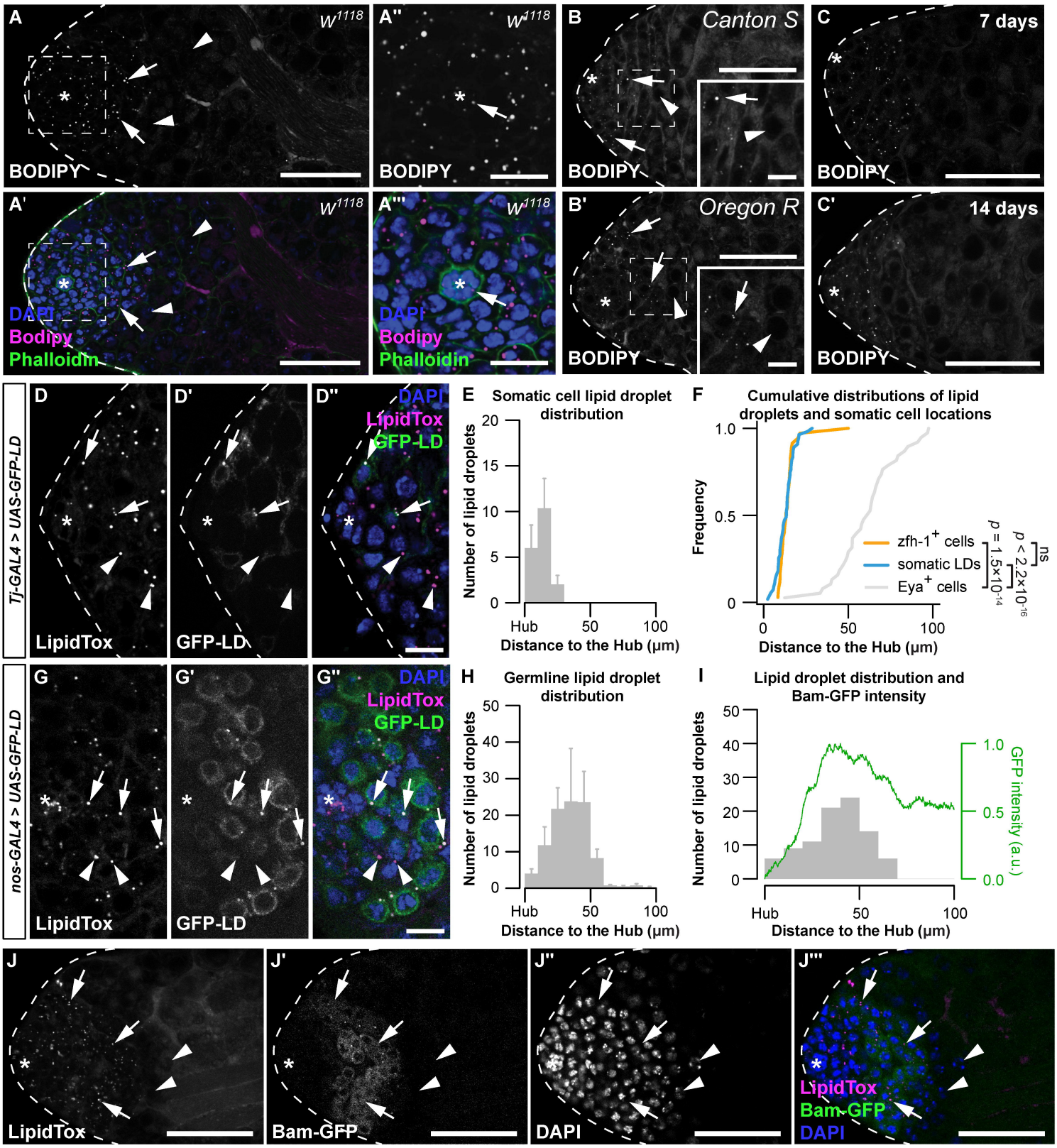
A
w1118
BODIPY
A''
w1118
BODIPY
B
Canton S
BODIPY
C
7 days
BODIPY
A'
w1118
DAPI
Bodipy
Phalloidin
A'''
w1118
DAPI
Bodipy
Phalloidin
B'
Oregon R
BODIPY
C'
14 days
BODIPY
Tj-GAL4 > UAS-GFP-LD
D
LipidTox
D'
GFP-LD
D''
DAPI
LipidTox
GFP-LD
E
Somatic cell lipid droplet distribution
Number of lipid droplets
Distance to the Hub (μm)
F
Cumulative distributions of lipid droplets and somatic cell locations
Frequency
zfh-1+ cells
somatic LDs
Eya+ cells
p = 1.5×10-14
p < 2.2×10-16
ns
Distance to the Hub (μm)
nos-GAL4 > UAS-GFP-LD
G
LipidTox
G'
GFP-LD
G''
DAPI
LipidTox
GFP-LD
H
Germline lipid droplet distribution
Number of lipid droplets
Distance to the Hub (μm)
I
Lipid droplet distribution and Bam-GFP intensity
Number of lipid droplets
GFP intensity (a.u.)
Distance to the Hub (μm)
J
LipidTox
J'
Bam-GFP
J''
DAPI
J'''
LipidTox
Bam-GFP
DAPI

FIGURE 1

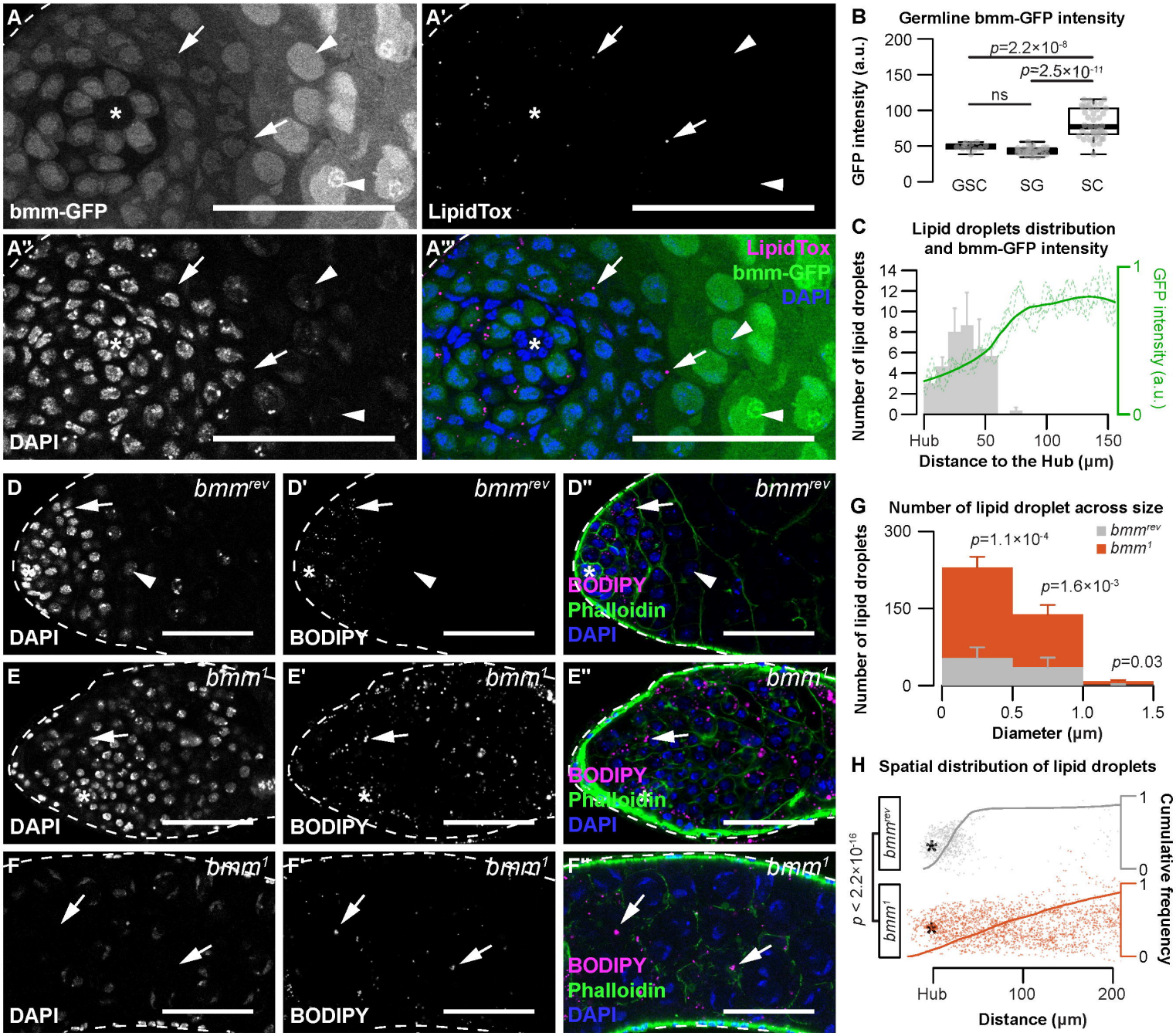
A
bmm-GFP
A'
LipidTox
A''
DAPI
A'''
LipidTox
bmm-GFP
DAPI
B
Germline bmm-GFP intensity
GFP intensity (a.u.)
p=2.2×10-8
p=2.5×10-11
ns
GSC
SG
SC
C
Lipid droplets distribution and bmm-GFP intensity
Number of lipid droplets
GFP intensity (a.u.)
Hub
Distance to the Hub (µm)
D
bmmrev
DAPI
D'
BODIPY
D''
BODIPY
Phalloidin
DAPI
E
bmm1
E'
E''
F
F'
F''
G
Number of lipid droplet across size
bmmrev
bmm1
p=1.1×10-4
p=1.6×10-3
p=0.03
Diameter (µm)
H
Spatial distribution of lipid droplets
p < 2.2×10-16
Cumulative frequency
Distance (µm)

FIGURE 2

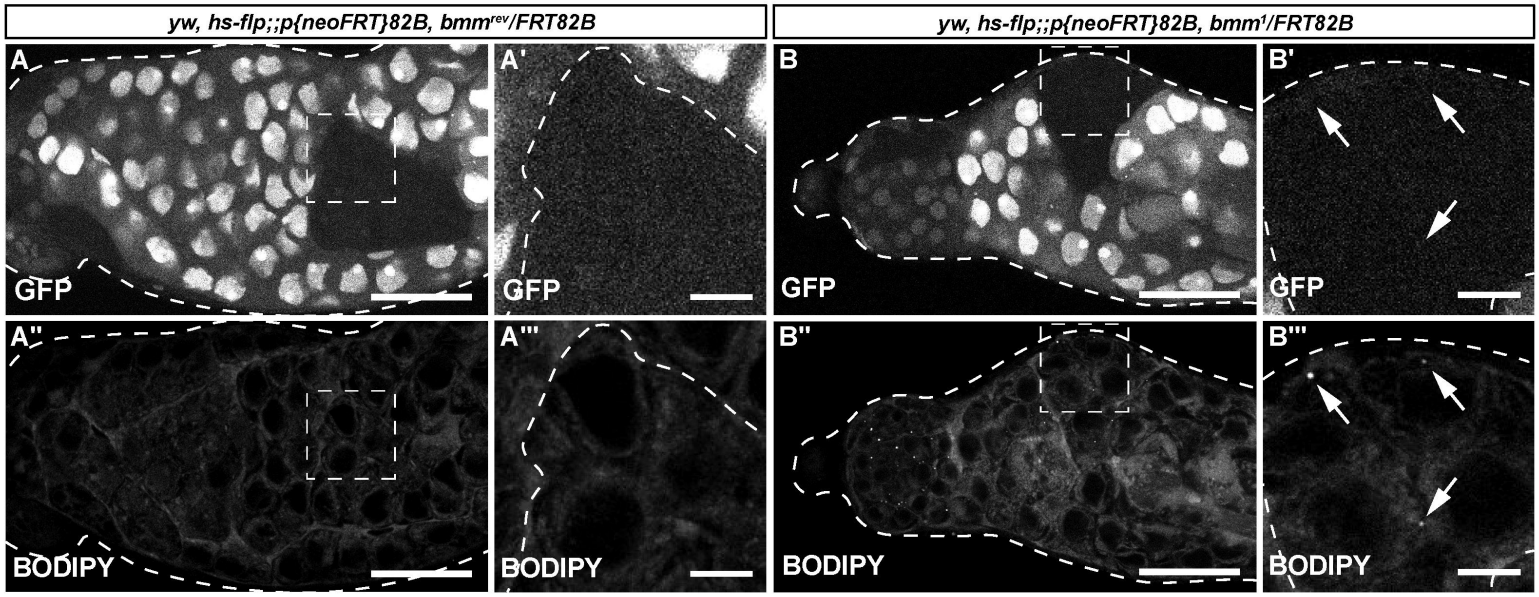
yw, hs-flp;;p{neoFRT}82B, bmm^rev/FRT82B
yw, hs-flp;;p{neoFRT}82B, bmm^1/FRT82B
A
A'
B
B'
GFP
A''
A'''
B''
B'''
BODIPY

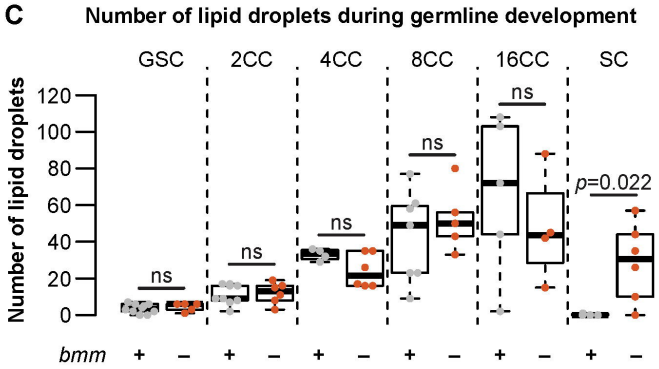
C
Number of lipid droplets during germline development
GSC
2CC
4CC
8CC
16CC
SC
Number of lipid droplets
120
100
80
60
40
20
0
ns
ns
ns
ns
ns
p=0.022
bmm
+
–

FIGURE 3

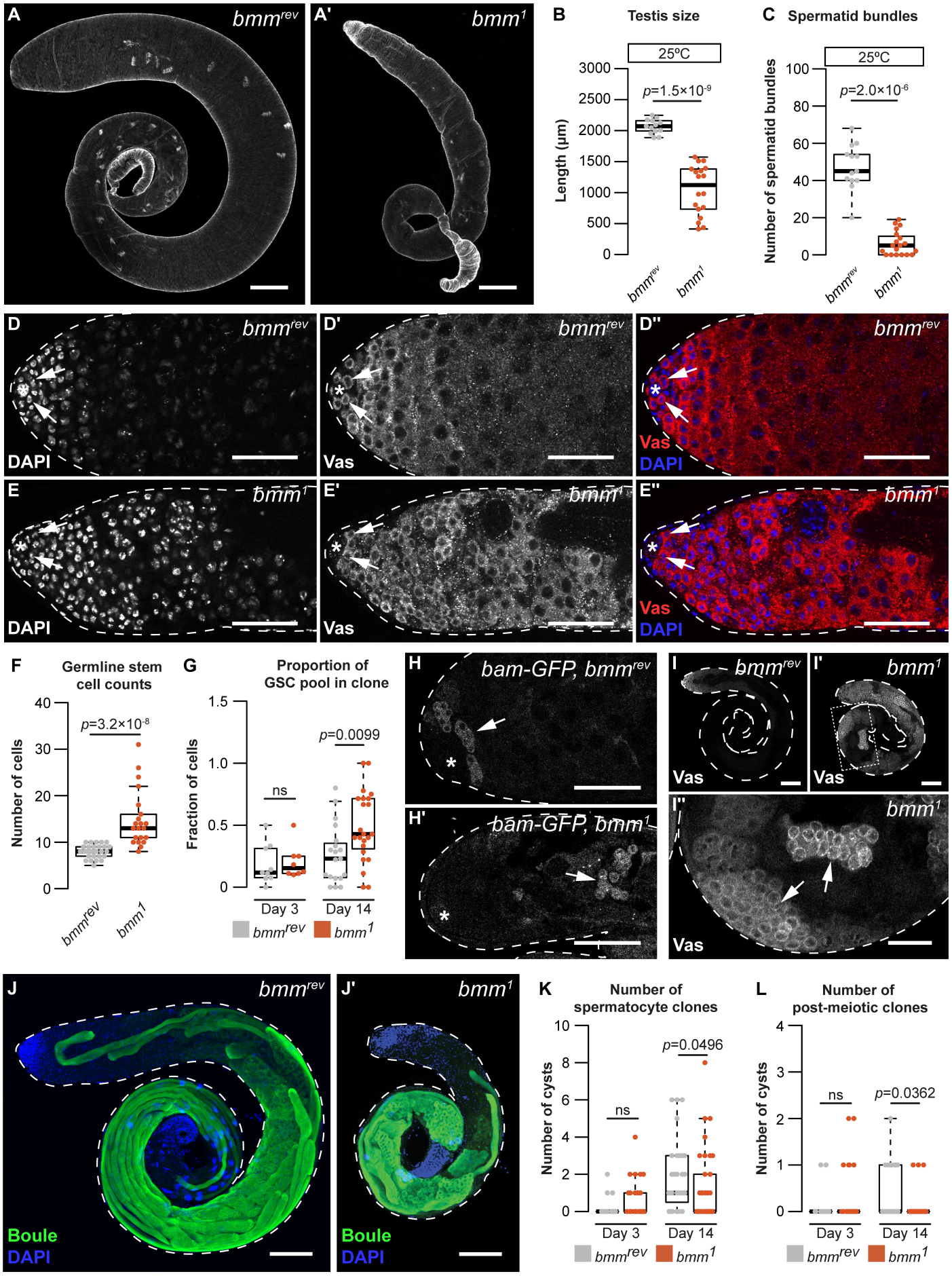
A
bmm^rev
A'
bmm^1
B
Testis size
25ºC
p=1.5×10^-9
Length (µm)
3000
2500
2000
1500
1000
500
0
bmm^rev
bmm^1
C
Spermatid bundles
25ºC
p=2.0×10^-6
Number of spermatid bundles
100
80
60
40
20
0
bmm^rev
bmm^1
D
bmm^rev
DAPI
D'
bmm^rev
Vas
D''
bmm^rev
Vas
DAPI
E
bmm^1
DAPI
E'
bmm^1
Vas
E''
bmm^1
Vas
DAPI
F
Germline stem cell counts
p=3.2×10^-8
Number of cells
40
30
20
10
0
bmm^rev
bmm^1
G
Proportion of GSC pool in clone
ns
p=0.0099
Fraction of cells
1.5
1.0
0.5
0
Day 3
Day 14
bmm^rev
bmm^1
H
bam-GFP, bmm^rev
H'
bam-GFP, bmm^1
I
bmm^rev
Vas
I'
bmm^1
Vas
I''
bmm^1
Vas
J
bmm^rev
Boule
DAPI
J'
bmm^1
Boule
DAPI
K
Number of spermatocyte clones
ns
p=0.0496
Number of cysts
10
8
6
4
2
0
Day 3
Day 14
bmm^rev
bmm^1
L
Number of post-meiotic clones
ns
p=0.0362
Number of cysts
4
3
2
1
0
Day 3
Day 14
bmm^rev
bmm^1

FIGURE 4

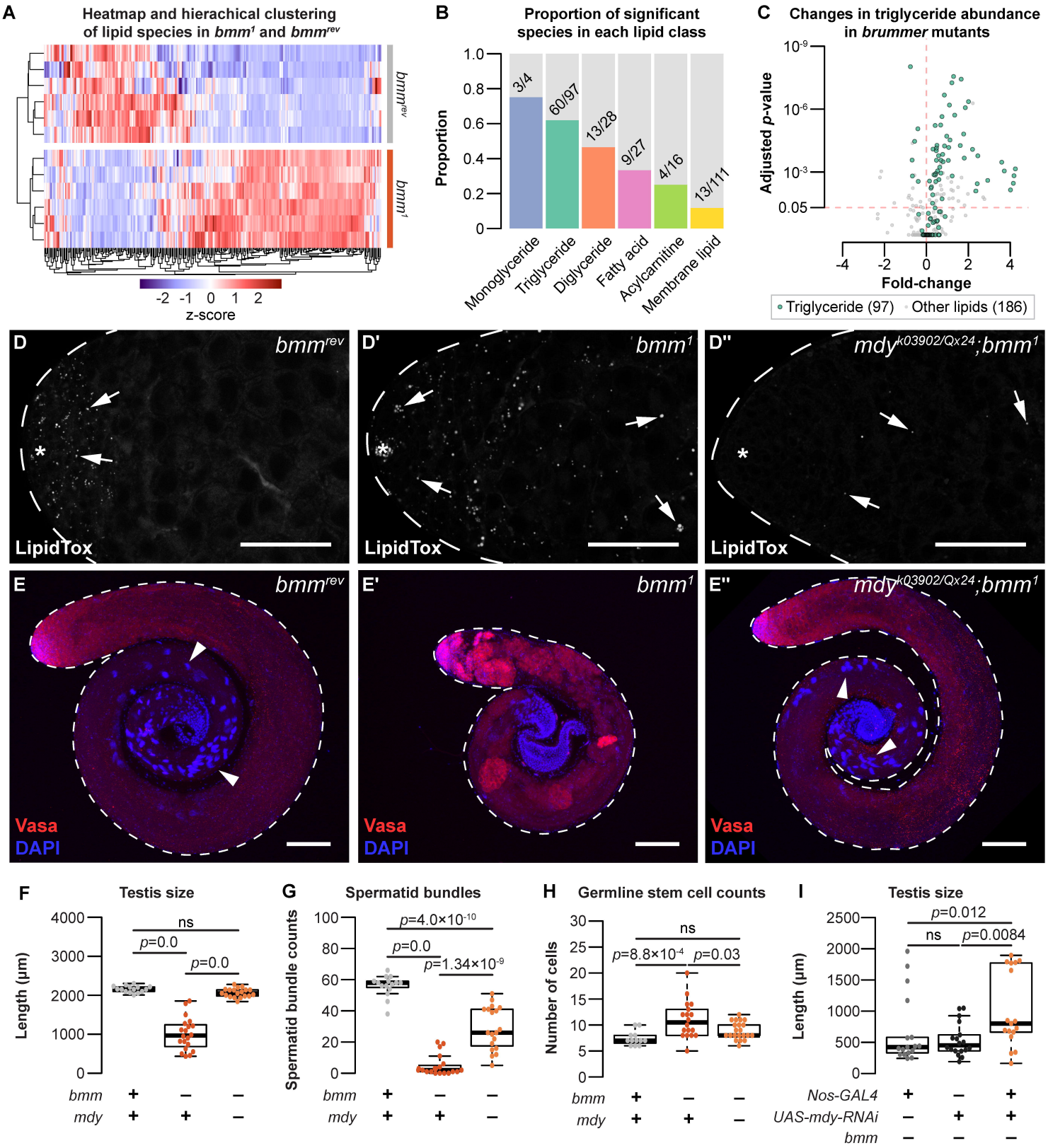
A
Heatmap and hierachical clustering of lipid species in bmm1 and bmmrev
bmmrev
bmm1
-2 -1 0 1 2
z-score
B
Proportion of significant species in each lipid class
Proportion
1.0
0.8
0.6
0.4
0.2
0
3/4
60/97
13/28
9/27
4/16
13/111
Monoglyceride
Triglyceride
Diglyceride
Fatty acid
Acylcarnitine
Membrane lipid
C
Changes in triglyceride abundance in brummer mutants
Adjusted p-value
10-9
10-6
10-3
0.05
-4 -2 0 2 4
Fold-change
Triglyceride (97)
Other lipids (186)
D
bmmrev
LipidTox
D'
bmm1
LipidTox
D''
mdyk03902/Qx24;bmm1
LipidTox
E
bmmrev
Vasa
DAPI
E'
bmm1
Vasa
DAPI
E''
mdyk03902/Qx24;bmm1
Vasa
DAPI
F
Testis size
Length (µm)
4000
3000
2000
1000
0
ns
p=0.0
p=0.0
bmm + – –
mdy + + –
G
Spermatid bundles
Spermatid bundle counts
100
80
60
40
20
0
p=4.0×10-10
p=0.0
p=1.34×10-9
bmm + – –
mdy + + –
H
Germline stem cell counts
Number of cells
30
25
20
15
10
5
0
ns
p=8.8×10-4
p=0.03
bmm + – –
mdy + + –
I
Testis size
Length (µm)
2500
2000
1500
1000
500
0
p=0.012
ns
p=0.0084
Nos-GAL4 + – +
UAS-mdy-RNAi – + +
bmm – – –

FIGURE 5

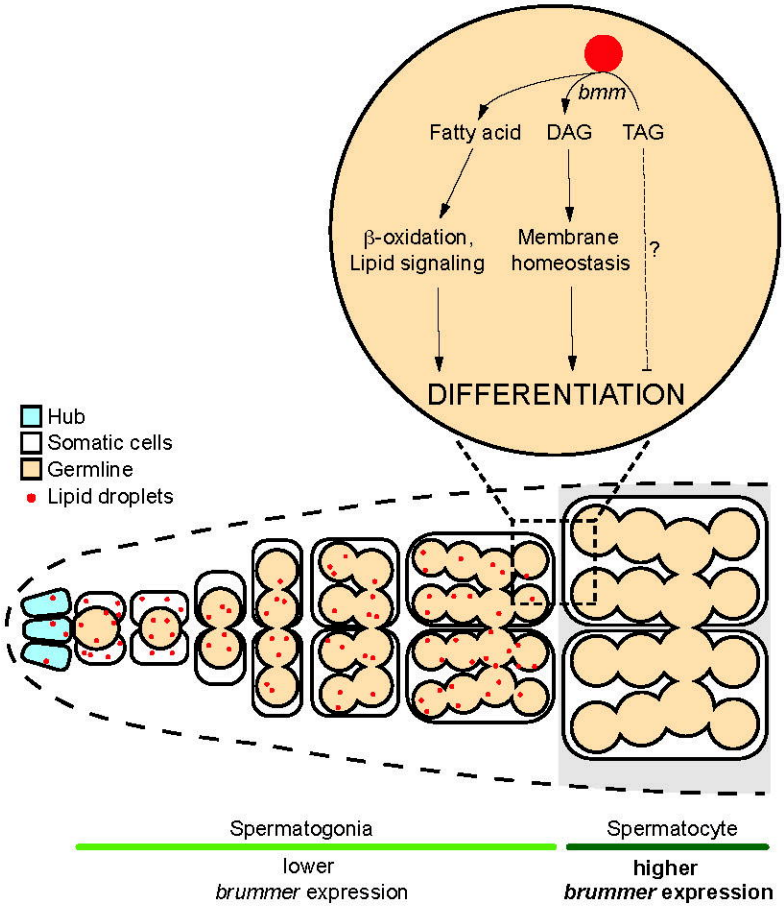
bmm
Fatty acid
DAG
TAG
β-oxidation,
Lipid signaling
Membrane
homeostasis
?
DIFFERENTIATION
Hub
Somatic cells
Germline
Lipid droplets
Spermatogonia
lower
brummer expression
Spermatocyte
higher
brummer expression

FIGURE 6

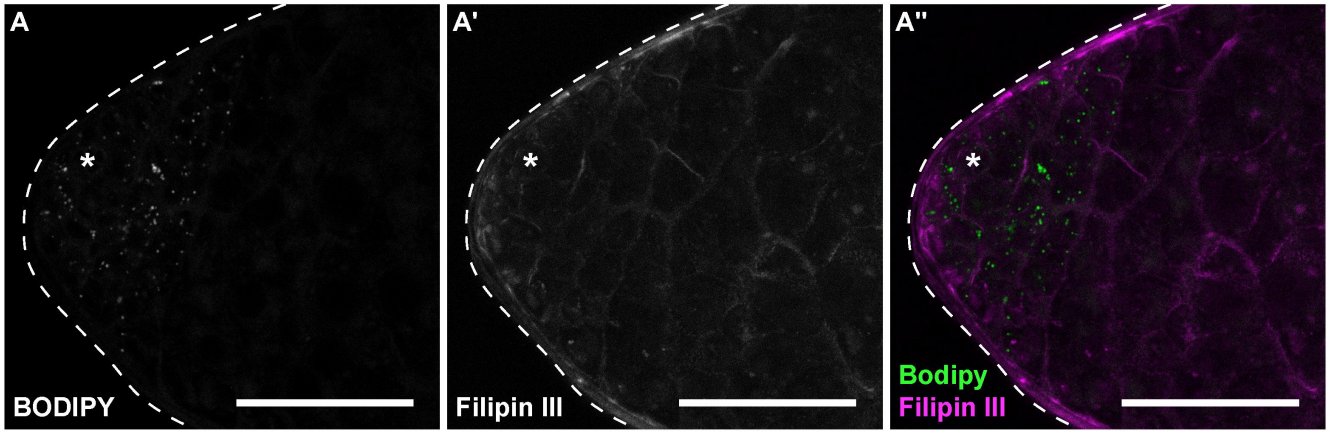

Supplemental figure 1 - related to Figure 1

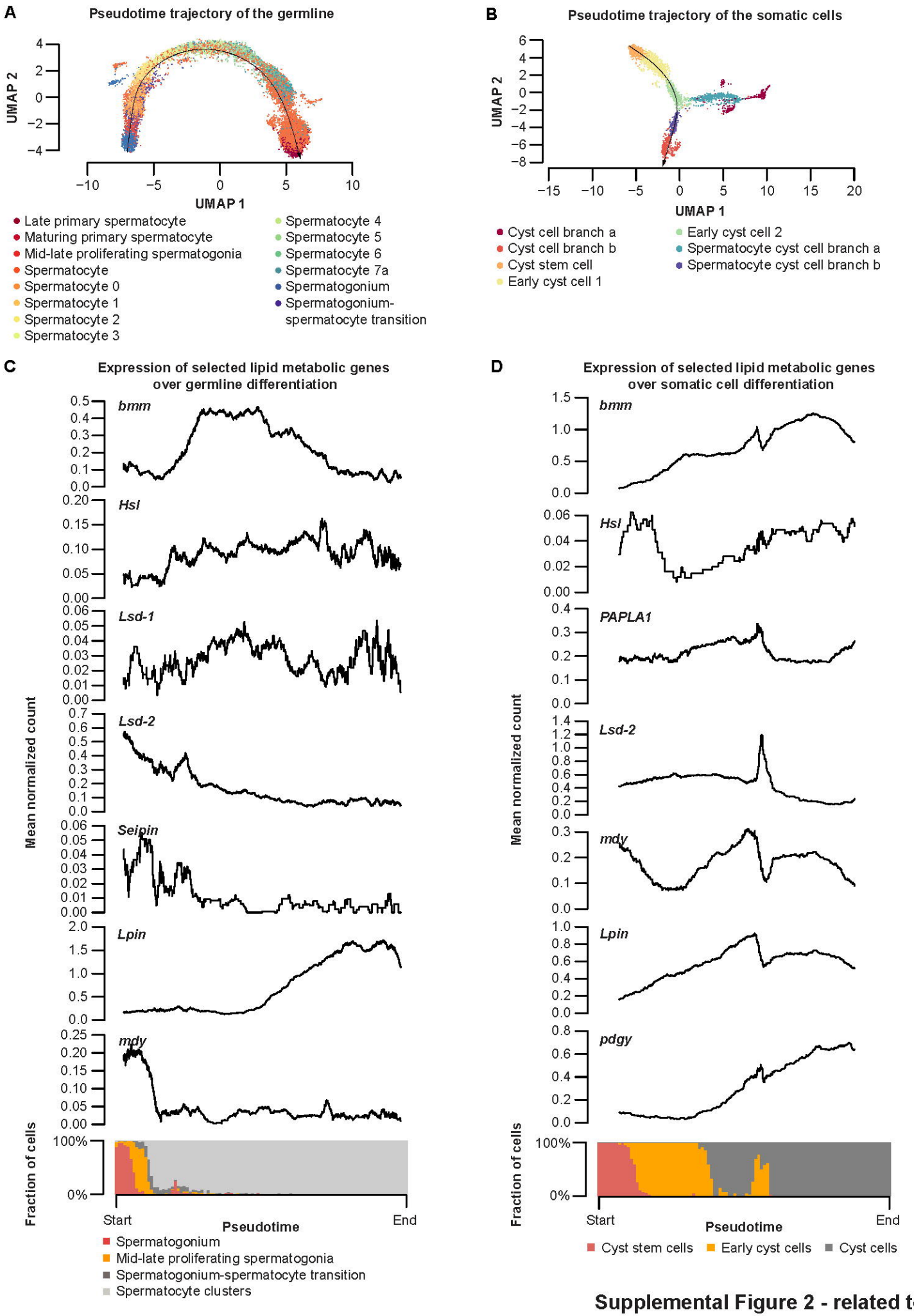

Supplemental Figure 2 - related to Figure 2

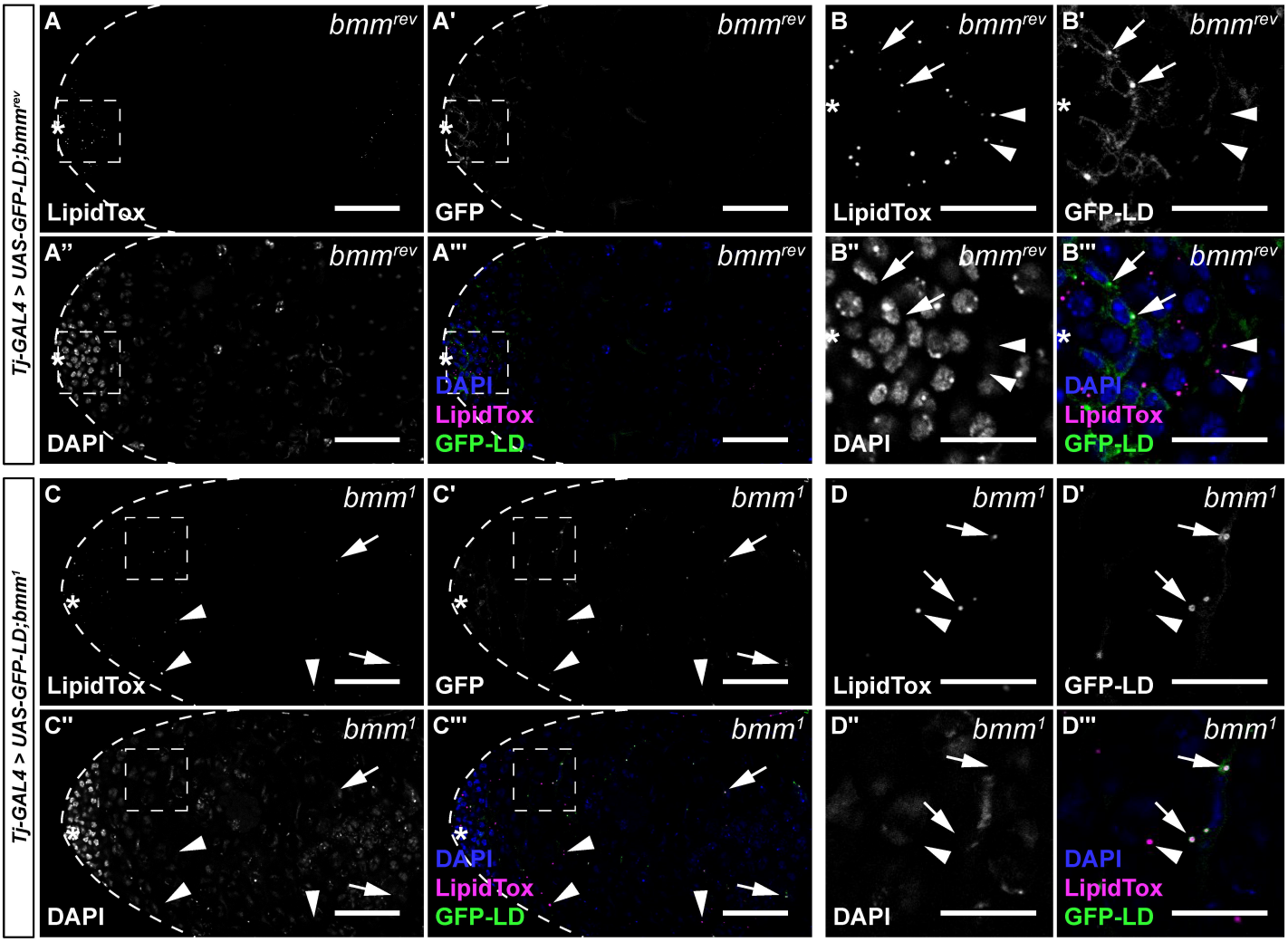

Supplemental figure 3 - related to Figure 2

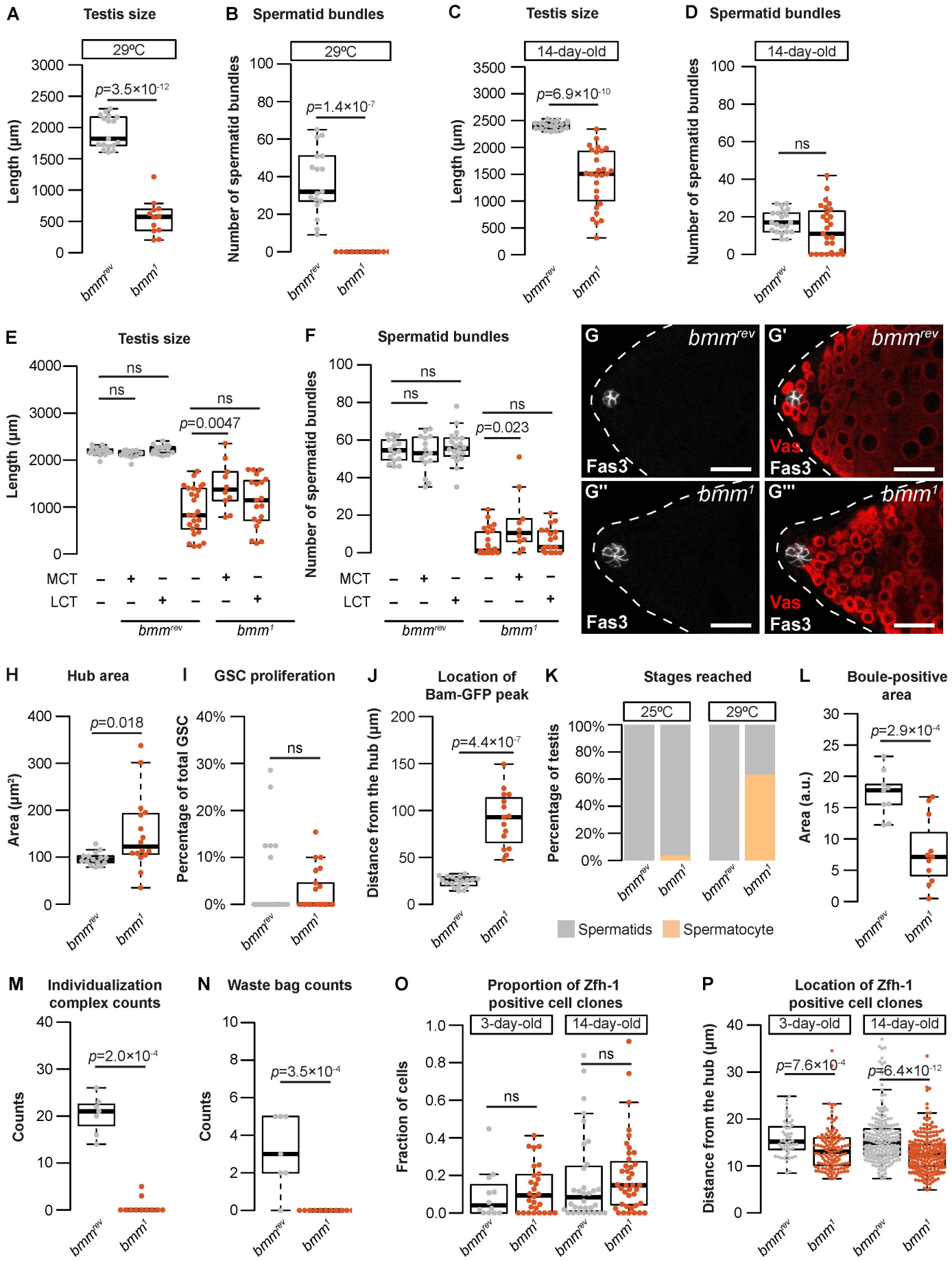

Supplemental figure 4 - related to Figure 4

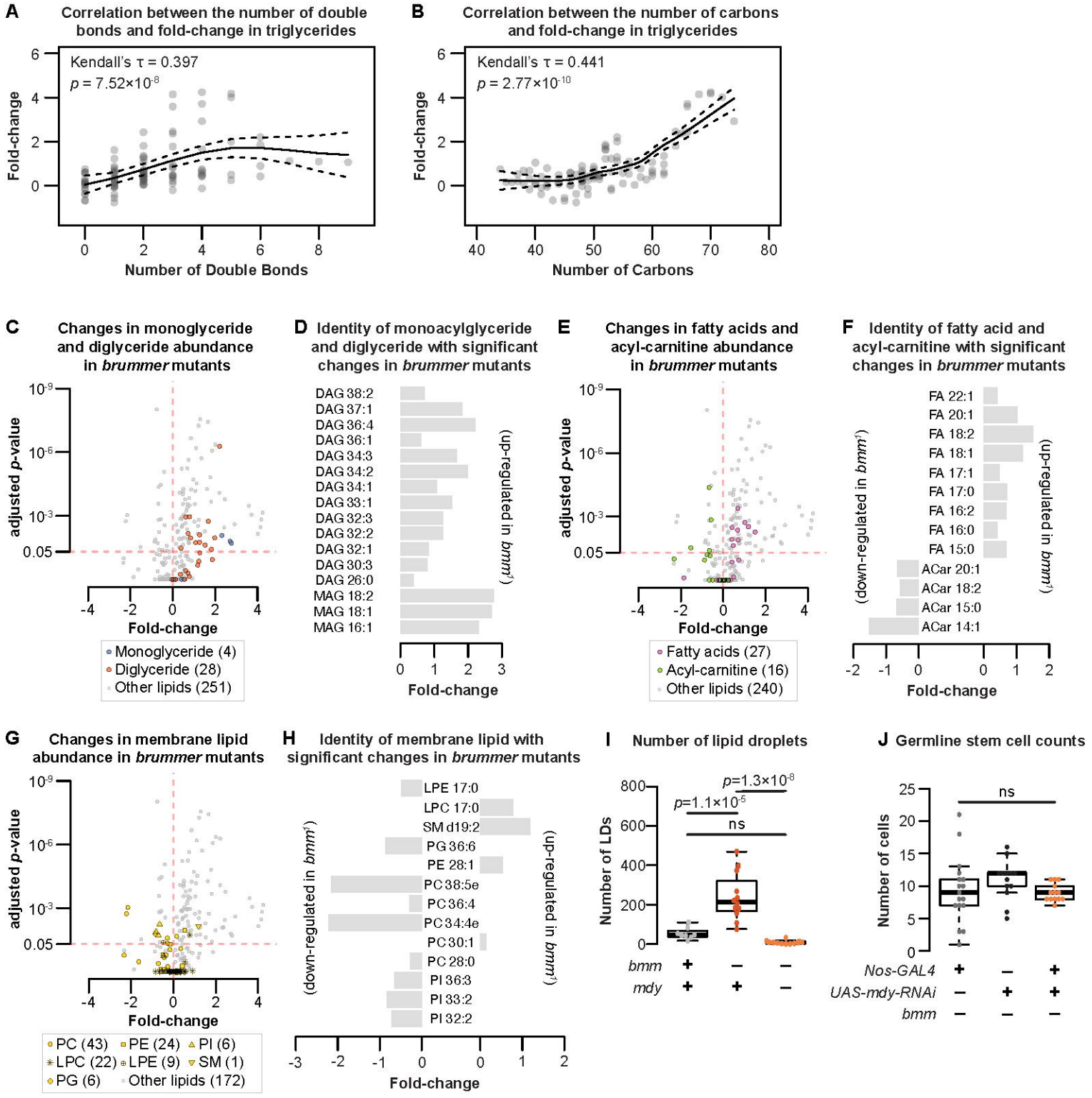

Supplemental figure 5 - related to Figure 5